5. Radiative Transfer in the (Expanding) Atmospheres of Early-Type Stars, and Related Problems

JOACHIM PULS

Abstract

In many cases, the quantitative spectroscopy of early-type stars requires to account for their line-driven winds, and theoretical models of such winds are based on a consistent calculation of the radiative line acceleration. Both topics ask for a thorough understanding of radiative transfer in expanding atmospheres. In this chapter, we concentrate on three issues, and compare, when possible, with corresponding results for plane-parallel, hydrostatic conditions: First, we investigate how sphericity alone affects the radiation field in those cases where Doppler shifts can be neglected (continua). Subsequently, we consider the impact of velocity fields on the line transfer, both by applying the so-called Sobolev approximation, and by presenting the more exact comoving-frame approach. Restrictions and extensions of both methods are discussed. Finally, we concentrate on the coupling between radiation field and occupation numbers via the NLTE rate equations. We illustrate the basic problem within the conventional lambda iteration, which is then solved by means of the so-called Accelerated Lambda Iteration (ALI), and by a 'preconditioning' of the rate equations.

5.1 (Very Brief) Introduction

One of the most striking observational features of early-type stars are their quasi-stationary UV P Cygni profiles (Figure 5.1), which indicate fast outflows, and, together with other diagnostics, only small variability of global quantities such as mass-loss rate, $\dot{M}$, and terminal velocity, v_∞.

These winds and their characteristic quantities have to be explained, diagnostic tools have to be developed, and predictions have to be given. All these tasks are comprised in the *theory of expanding atmospheres*[1].

Beginning with the theoretical work by Lucy and Solomon (1970) and Castor et al. (1975, "CAK"), it turned out that the winds from early-type stars are driven by radiative line acceleration, and subsequent diagnostics revealed that typical mass-loss rates lie in the range $10^{-7}\ldots10^{-5} M_\odot \mathrm{yr}^{-1}$, with v_∞ between 200 and 3,000 $\mathrm{km\,s}^{-1}$, fairly proportional to the corresponding photospheric escape speeds.[2]

In order to account for the presence of these winds when synthesizing theoretical spectral energy distributions (SEDs) (quantitative spectroscopy!), and to enable the calculation of the line acceleration required to set up theoretical models, the *radiative transfer in expanding media* needs to be formulated and understood, which is the topic of the following chapter. Particularly, there are two effects that give rise to major differences compared to plane-parallel, hydrostatic calculations used, e.g., for the analysis of late-type

[1] In addition to the references provided in the following, we also recommend the textbooks by Mihalas (1978) and Hubený and Mihalas (2014).

[2] For specific reviews on the topic of line-driven winds, see Kudritzki and Puls (2000) and Puls et al. (2008).

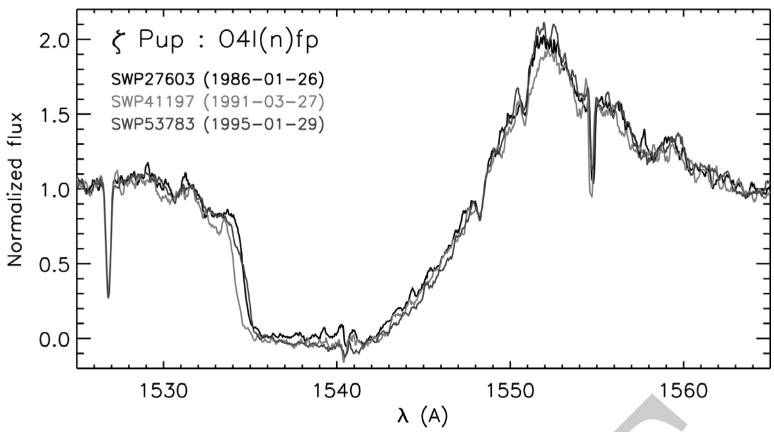

FIGURE 5.1. Three UV P Cgyni profiles of the C IV resonance line from the O4 supergiant ζ Pup obtained (several years apart) with the International Ultraviolet Explorer (IUE) space mission. Note how the overall shape of the spectrum (indicating a terminal velocity, v_∞, of roughly 2,500 km s^{-1}) remains fairly constant.

stars (see Chapters 2 and 6): *sphericity*, which affects the radiation field and (wind-) density, to be covered in Sections 5.2 and 5.3, and *velocity fields*, which mostly affect the line transfer, via the induced Doppler shifts, to be discussed in Section 5.4.

5.2 From p-p Symmetry to Spherical Atmospheres with Velocity Fields

As long as $\Delta r/R_* \ll 1$, with Δr the vertical extent of the atmosphere and R_* the stellar radius, plane-parallel (p-p) symmetry can be assumed, at least in a 1-D treatment. Such an approach is valid, e.g., for the solar photosphere, when refraining from a precise description of convection. Since the curvature of the stellar atmosphere is neglected in a p-p approach, the angle between a photon's path and the isocontours of important quantities such as density and temperature remains constant throughout the atmosphere. On the other hand, when $\Delta r/R_* \gtrsim 1$, as in the solar corona or in the winds of early-type stars or red giants/supergiants, at least spherical symmetry needs to be adopted, but in any case the aforementioned angle changes drastically when propagating from the bottom to the top of the atmosphere.

5.2.1 *Coordinate Systems and Symmetries*

When using a cartesian coordinate system, a vector $\mathbf{r}$ is expressed via $\mathbf{r} = x\mathbf{e}_x + y\mathbf{e}_y + z\mathbf{e}_z$, while in a spherical coordinate system $\mathbf{r} = \Theta\mathbf{e}_\Theta + \Phi\mathbf{e}_\Phi + r\mathbf{e}_r$, where $\mathbf{e}_x$, $\mathbf{e}_y$, $\mathbf{e}_z$ and $\mathbf{e}_\Theta$, $\mathbf{e}_\Phi$, $\mathbf{e}_r$ form a right-handed, orthonormal base. In such systems, the specific intensity depends on $I(x, y, z, t; \mathbf{n}, \nu)$ and $I(\Theta, \Phi, r, t; \mathbf{n}, \nu)$, respectively, where $\mathbf{n}$ is the direction vector, ν the frequency, and t the time. Related symmetries are the plane-parallel one, where all physical quantities depend only on z, e.g., $I(\mathbf{r}, t; \mathbf{n}, \nu) \to I(z, t; \mathbf{n}, \nu)$, and the spherical symmetry, with physical quantities depending only on r, e.g., $I(\mathbf{r}, t; \mathbf{n}, \nu) \to I(r, t; \mathbf{n}, \nu)$.

Since the specific intensity has direction $\mathbf{n}$ into dΩ, additional angles θ, ϕ with respect to $(\mathbf{e}_x, \mathbf{e}_y, \mathbf{e}_z)$ or $(\mathbf{e}_\Theta, \mathbf{e}_\Phi, \mathbf{e}_r)$ are required, with polar angle, $\theta = \sphericalangle(\mathbf{e}_z, \mathbf{n})$ or $\theta = \sphericalangle(\mathbf{e}_r, \mathbf{n})$, respectively (see Figure 5.2). Thus, I_ν can be expressed as $I_\nu(x, y, z, t; \theta, \phi)$ or $I_\nu(r, \Theta, \Phi, t; \theta, \phi)$.

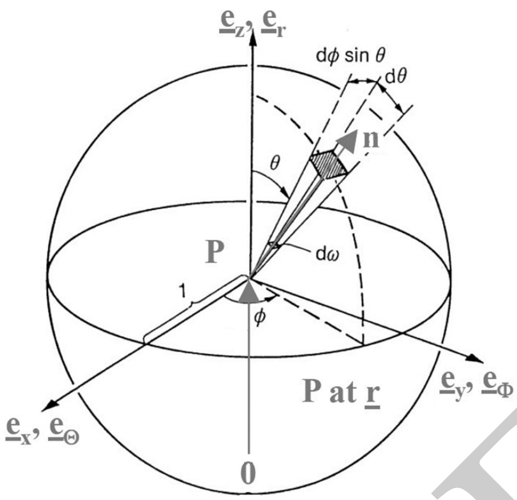

FIGURE 5.2. Directional angles, θ, ϕ, and solid angle element $\mathrm{d}\Omega = \mathrm{d}\phi \sin\theta \times \mathrm{d}\theta$, as used to calculate the specific intensity $I_\nu(\mathbf{r}, \mathbf{n}, t)$ at point P, for both a cartesian and a spherical coordinate system (see text).

Both in plane-parallel and spherical symmetry, the intensity does not dependent on azimuthal direction, ϕ (again Figure 5.2), and we finally obtain $I_\nu \rightarrow I_\nu(z, t; \theta)$ or $\rightarrow I_\nu(r, t; \theta)$, respectively.

5.2.2 *Hydrostatic Equilibrium*

In plane-parallel atmospheres without winds (e.g., Kurucz atmospheres), but also in atmospheric models aiming at a description of early-type stars with thin winds (e.g., TLUSTY or DETAIL/SURFACE; see Appendix A); the pressure/density stratification is conventionally prescribed assuming hydrostatic equilibrium, namely

$$\frac{\partial P}{\partial z} = \rho(z) \left(-g_{\mathrm{grav}} + g_{\mathrm{rad}}(z)\right), \tag{5.1}$$

where $g_{\mathrm{grav}} = GM_*/R_*^2$ and again $\Delta z(\text{photosphere}) \ll R_*$. Integration of (5.1) gives either

$$P_{\mathrm{tot}}(z) = g_{\mathrm{grav}} \cdot m,$$

where $P_{\mathrm{tot}} = P_{\mathrm{gas}} + P_{\mathrm{rad}}$ and the mass column density is defined as $m \equiv \int_z^\infty \rho(z) dz$, or, neglecting g_{rad} and adopting a constant surface temperature T_*,

$$\rho(z) \approx \rho(z=0)\ e^{-z/H},$$

with photospheric scale height

$$H = \frac{k_{\mathrm{B}} T_*}{\mu\ m_{\mathrm{H}}\ g_{\mathrm{grav}}} = \frac{2\ v_{\mathrm{sound}}^2(T_*)}{v_{\mathrm{esc}}^2}\ R_*.$$

Here $v_{\mathrm{sound}} = \sqrt{k_{\mathrm{B}} T/\mu\ m_{\mathrm{H}}}$ is the isothermal speed of sound (of order of few $\mathrm{km\,s^{-1}}$), μ the mean molecular weight, and $v_{\mathrm{esc}} = \sqrt{2GM_*/R_*}$ the photospheric escape velocity (usually of order of several 100 $\mathrm{km\,s^{-1}}$). Alternatively, neglecting again g_{rad},

$$\rho(m) \approx \frac{1}{H} m, \quad \text{i.e.,} \qquad \log\rho = \log m - \log H. \tag{5.2}$$

When velocity fields are taken into account, conservation of mass leads to the *equation of continuity*

$$\frac{\partial \rho}{\partial t} + \nabla \cdot (\rho \mathbf{v}) = 0,$$

which for a steady one-dimensional spherical flow reduces to

$$4\pi\, r^2 \rho\, v = \text{const } = \dot{M}, \tag{5.3}$$

where $\dot{M}$ is the (constant) mass-loss rate through a spherical surface.

From the conservation of momentum, one obtains Euler's equation

$$\frac{\partial \rho}{\partial t} + \nabla \cdot (\rho \mathbf{v}\mathbf{v}) = -\nabla P + \rho\, \mathbf{g}^{\text{ext}}. \tag{5.4}$$

By $\mathbf{vv}$ we denote the dyadic product, and $\mathbf{g}^{\text{ext}}$ the total external acceleration. From vector calculus it holds that $\nabla \cdot (\rho \mathbf{vv}) = \mathbf{v}\, [\nabla \cdot (\rho \mathbf{v})] + [\rho \mathbf{v} \cdot \nabla]\, \mathbf{v}$. For a one-dimensional spherical flow, (5.4) reduces to the *equation of motion*

$$\rho\, v\, \frac{\partial v}{\partial r} = -\frac{\partial P}{\partial r} + \rho\, g_r^{\text{ext}}. \tag{5.5}$$

The LHS of (5.5) is the advection term due to inertia. The comparison of (5.5) – where gravity and radiative acceleration are taken into account – with (5.1), namely

$$\frac{\partial P}{\partial r} = \rho(r) \left(-\frac{G M_*}{r^2} + g_{\text{rad}}(r) \right) - \rho(r) v(r)\, \frac{\partial v}{\partial r}$$

and

$$\frac{\partial P}{\partial z} = \rho(z) \left(-\frac{G M_*}{R_*^2} + g_{\text{rad}}(z) \right),$$

shows the importance of the advection term.

5.2.3 *When Is a (Quasi-)Hydrostatic Approach Justified?*

By using the equation of state $P = (k_{\text{B}} T / \mu m_{\text{H}}) \rho = v_{\text{sound}}^2\, \rho$ and the equation of continuity (5.3), the equations of motion and of hydrostatic equilibrium can be rewritten as follows:

$$\left(v_{\text{sound}}^2(r) - v^2(r)\right) \frac{\partial \rho}{\partial r} = -\rho(r) \left(g_{\text{grav}}(r) - g_{\text{rad}}(r) + \frac{\mathrm{d} v_{\text{sound}}^2}{\mathrm{d} r} - \frac{2 v^2(r)}{r} \right) \text{[hydrodyn.]}$$

$$v_{\text{sound}}^2(z) \frac{\partial \rho}{\partial z} = -\rho(z) \left(g_{\text{grav}}(R_*) - g_{\text{rad}}(z) + \frac{\mathrm{d} v_{\text{sound}}^2}{\mathrm{d} z} \right) \quad \text{[hydrostatic]}.$$

By comparing both equations, we note that the 'only' difference is an additional term $\propto v^2$ both on the left and right side of the equation of motion, and we conclude that for $v \ll v_{\text{sound}}$ – i.e., in deeper photospheric regions, well below the sonic point where $v(r_{\text{S}}) = v_{\text{sound}}$ – the hydrodynamic density stratification approaches the (quasi-)hydrostatic one.

Thus, p-p atmospheres using hydrostatic equilibrium yield reasonable results *even in the presence of winds*, as long as the studied features (continua, lines) are formed below the sonic point (see also the following subsection).

5.2.4 *Unified Atmospheres*

The concept of 'unified atmospheres' (= wind + photosphere) was founded by Gabler et al. (1989). Nowadays, two flavors of such a description are present:

(a) The complete stratification is adapted from theoretical wind models based on the (modified) CAK theory (Friend and Abbott, 1986; Pauldrach et al., 1986), such that either $\dot{M}$ and v_∞ of the models agree with the required input values, or the stratification results from a self-consistent calculation w.r.t. $g_{\rm rad}$ (without the possibility to choose arbitrary combinations of wind and stellar parameters as input). Both methods are used within the atmosphere code WM-basic (Pauldrach et al., 2001). The disadvantage of this approach is that it is difficult (or even impossible) to manipulate the density/velocity stratification in case the theory is not applicable or too simplified.

(b) A quasistatic photosphere is combined with an empirical wind structure (PoWR, CMFGEN, PHOENIX, FASTWIND; see Appendix A), with the disadvantage that the transition region is somewhat ill defined. Specifically, in deep layers $\rho(r)$ is calculated from (quasi-)hydrostatic equilibrium (5.1) (with R_* replaced by r), and the corresponding velocity is derived via

$$v(r) = \frac{\dot{M}}{4\pi r^2 \rho(r)} \qquad \text{for } v \ll v_{\rm sound} \qquad (\text{roughly: } v < 0.1 v_{\rm sound}).$$

In the outer layers, at first $v(r)$ is defined using the semi-empirical 'beta velocity law' for radiation driven winds (e.g., Pauldrach et al. 1986, and Figure 5.3),

$$v(r) = v_\infty \Big(1 - \frac{bR_*}{r}\Big)^\beta, \tag{5.6}$$

with $0.5 < \beta \lesssim 2 \ldots 3$, and b derived from the transition velocity. In this regime, then, the density results from

$$\rho(r) = \frac{\dot{M}}{4\pi r^2 v(r)}.$$

Finally, a certain transition zone is defined to ensure a smooth transition from the deeper to the outer layers. This unified description is quite flexible, and the corresponding input/fit parameters are $\dot{M}$, v_∞, β, and the transition velocity. A comparison of a hydrostatic and unified atmospheric structure is presented in Figure 5.4. We stress that at the same $\tau_{\rm Ross}$ or m, the wind density (for $v \gtrsim v_{\rm sound}$) is *lower* than the hydrostatic one.

5.2.5 *Plane-Parallel or Unified Atmospheres?*

Since the calculation of unified atmospheres plus corresponding SEDs is much more time consuming than the calculation of plane-parallel ones, it is reasonable to check beforehand which approach is required. Accounting for the formation region of optical lines (see Figure 5.4), unified models become vital if $\tau_{\rm Ross} \gtrsim 10^{-2}$ at the transition between photosphere and wind (roughly located at $0.1 v_{\rm sound}$). Using a typical velocity law ($\beta = 1$), as a rule of thumb

$$\dot{M}_{\rm max} = \dot{M}(\tau_{\rm Ross} = 10^{-2} \text{ at } 0.1 v_{\rm sound}) \approx 6 \cdot 10^{-8} M_\odot {\rm yr}^{-1} \cdot \frac{R_*}{10\,R_\odot} \cdot \frac{v_\infty}{1000\,{\rm km\,s^{-1}}}.$$

If the actual $\dot{M} < \dot{M}_{\rm max}$ for the considered object, most diagnostic features are formed in the quasihydrostatic part of the atmosphere, and plane-parallel models can be used.

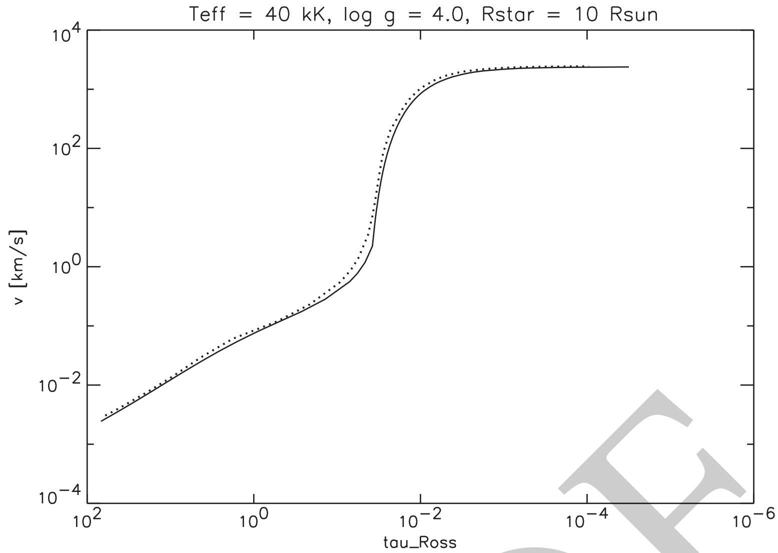

FIGURE 5.3. Velocity fields for unified O-star models with a comparatively thin wind. Dotted: hydrodynamic solution following Pauldrach et al. (1986); solid: analytical velocity law (5.6) with similar terminal velocity and $\beta = 0.8$, extended towards larger depths using a quasihydrostatic approach.

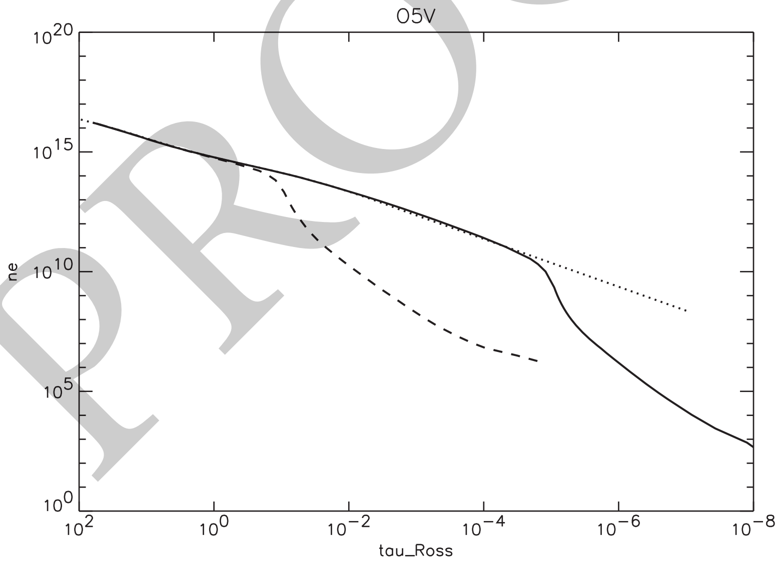

FIGURE 5.4. Electron density as a function of τ_{Ross}, for different atmospheric models of an O5-dwarf. Dotted: hydrostatic model atmosphere, cf. (5.2); solid, dashed: unified models with a thin and a moderately dense wind, respectively. In case of the denser wind, the cores of the optical lines ($\tau_{\mathrm{Ross}} \approx 10^{-1} - 10^{-2}$) are formed at significantly different densities than in the hydrostatic model, whereas the unified, thin-wind model and the hydrostatic one would lead to similar results.

Typically, this refers to the optical spectroscopy of late O-dwarfs and B-stars up to luminosity class II (for early subtypes) or Ib (mid/late subtypes).

5.3 Radiative Transfer: From p-p to Spherical Symmetry

5.3.1 *Basic Considerations*

In the following, we will mostly restrict ourselves to 1-D problems, since multi-D problems are beyond the scope of this overview. At first we will summarize the major changes in the description/properties of the radiation field when switching from a plane-parallel to a spherically symmetric situation.

Basically, the specific intensity and its moments are similarly defined when proceeding from the p-p height coordinate, z, to the radial distance, r.

$$I(z,\mu) \rightarrow I(r,\mu) \text{ with } \mu = \cos\theta \text{ and } \theta = \sphericalangle(\mathbf{e}_r, \mathbf{n}),$$

where here and in the following notation, the ν and t dependence has been suppressed. From the adopted symmetry (independence from the azimuthal direction, e.g., Figure 5.2), the nth moment of the specific intensity, namely

$$M_n = \frac{1}{2}\int_{-1}^{+1} I(r,\mu)\mu^n \mathrm{d}\mu,$$

is equally defined as in the p-p case when $z \rightarrow r$. For $n = 0,1,2$, we obtain the mean intensity, the Eddington flux and the second moment, $J(r)$, $H(r)$ and $K(r)$, respectively. The flux(-density) vector,

$$\mathcal{F} = \big(0, 0, 4\pi H\big)^T,$$

has only an r-component different from zero, which is proportional to the Eddington flux.

Regarding the radiation stress tensor, $\mathbf{P}$, only the diagonal elements are different from zero (as in the p-p case), and the only difference thus far refers to the divergence of the stress tensor (which is related to the radiation force; see (5.11)). While in p-p symmetry, only its z-component is different from zero, and

$$\left(\nabla \cdot \mathbf{P}\right)_z = \frac{\partial p_\mathrm{R}}{\partial z}, \text{ with } p_\mathrm{R} \text{ (radiation pressure scalar) } = \frac{4\pi}{c}K(z),$$

in spherical symmetry only the r-component is different from zero, and

$$\left(\nabla \cdot \mathbf{P}\right)_r = \frac{\partial p_\mathrm{R}}{\partial r} + \frac{3p_\mathrm{R} - u}{r}\text{ , with } u \text{ (radiation energy density) } = \frac{4\pi}{c}J(r).$$

Behaviour at large distances from the surface: optically thin envelopes. An important difference between p-p and spherically symmetric configurations relates to the behaviour of the radiation field at large distances from the stellar surface, which in case of spherical symmetry is affected by geometrical dilution. To estimate corresponding effects, let's assume an optically thin envelope, i.e., $I_\nu(r) :=$ const for a specific ray, and that the radiation field leaving the effective photosphere, R_eff, is isotropic: $I_\nu^{+,\mathrm{phot}}(R_\mathrm{eff},\mu) :=$ const $= I_\nu^+(R_\mathrm{eff})$:

$$\Rightarrow M_n = \frac{1}{2}\int_{-1}^{+1} I_\nu(\mu)\mu^n \mathrm{d}\mu \quad \rightarrow \quad \frac{1}{2}\int_{\mu_*}^{+1} I_\nu^+(R_\mathrm{eff})\mu^n \mathrm{d}\mu = \frac{1}{2}I_\nu^+(R_\mathrm{eff})\frac{\left(1-\mu_*^{n+1}\right)}{n+1}.$$

In this case, for the 0th moment we find $J_\nu \approx W I_\nu^+(R_{\rm eff})$, with dilution factor

$$W = \frac{1}{2}(1 - \mu_*) \text{ and } \mu_* = \sqrt{1 - \left(\frac{R_{\rm eff}}{r}\right)^2} \tag{5.7}$$

where μ_* is the cosine of the (half) cone angle subtended by stellar disk, θ_*, which can be calculated via $\sin\theta_* = R_{\rm eff}/r$. Now, for $r \gg R_{\rm eff}$,

$$\mu_*^{n+1} \to \left(1 - \frac{n+1}{2}\left(\frac{R_{\rm eff}}{r}\right)^2\right),$$

and *any* moment

$$J_\nu = H_\nu = K_\nu = \ldots . \to \quad \frac{1}{4} I_\nu^+(R_{\rm eff})\left(\frac{R_{\rm eff}}{r}\right)^2.$$

In other words, all moments become equal, and the Eddington factors (ratios of moments) converge to unity for $r \gg R_{\rm eff}$. This is specific for (spherical) envelopes at large distances, and different from corresponding plane-parallel results. (Exercise: perform the same calculation for plane-parallel conditions and large z.)

The equation of radiative transfer (RTE). Independent from any coordinate system and discarding general relativity (GR) effects, the RTE reads

$$\left(\frac{1}{\rm c}\frac{\partial}{\partial t} + \mathbf{n}\cdot\nabla\right) I_\nu(\mathbf{r},\mathbf{n},t) = \eta_\nu(\mathbf{r},\mathbf{n},t) - \chi_\nu(\mathbf{r},\mathbf{n},t) I_\nu(\mathbf{r},\mathbf{n},t), \tag{5.8}$$

where η_ν is the total emissivity, χ_ν the total opacity, and $\mathbf{n}\cdot\nabla$ the directional derivative $\triangleq \frac{\rm d}{{\rm d}s}$ along path s.

In plane-parallel geometry, $\mathbf{n}\cdot\nabla \to \mu{\rm d}/{\rm d}z$, since the actual path is longer than the height difference, ${\rm d}s = {\rm d}z/\mu$, and we obtain, when discarding the time-dependence for stationary conditions,

$$\mu\frac{\rm d}{{\rm d}z} I_\nu(z,\mu) = \eta_\nu(z,\mu) - \chi_\nu(z,\mu) I_\nu(z,\mu) \quad \text{(plane-parallel, stationary).}$$

In spherical geometry, μ is no longer constant along a certain direction $\mathbf{n}$. Restricting ourselves to spherical symmetry,

$$\mathbf{n}\cdot\nabla \Rightarrow \mu\frac{\partial}{\partial r} + \frac{(1-\mu^2)}{r}\frac{\partial}{\partial\mu},$$

which can be shown by using the so-called p-z geometry (see the following section). For stationary processes, we then have

$$\left(\mu\frac{\partial}{\partial r} + \frac{(1-\mu^2)}{r}\frac{\partial}{\partial\mu}\right) I_\nu(r,\mu) = \eta_\nu(r,\mu) - \chi_\nu(r,\mu) I_\nu(r,\mu) \quad \text{(sph. symm., stationary).}$$

Moments of the RTE. The zero- and first-order-moment equations are obtained by integrating the RTE over ${\rm d}\Omega$ or by multiplying with $\mathbf{n}/c$ and integrating over ${\rm d}\Omega$, respectively, and are very useful and insightful for many problems/applications.

In the general case, the zero-order-moment equation reads

$$\frac{4\pi}{\rm c}\frac{\partial}{\partial t} J_\nu + \nabla\cdot\mathcal{F}_\nu = \oint (\eta_\nu - \chi_\nu I_\nu)\,{\rm d}\Omega. \tag{5.9}$$

After integrating over frequency, the RHS of this equation becomes zero ('radiative equilibrium'), as long as only radiation energy is transported. For time-independent problems, this then refers to 'flux-conservation', $\nabla \cdot \mathcal{F} = 0$, with $\mathcal{F}$ the *total* flux.

For plane-parallel, stationary and static conditions, (5.9) collapses to

$$\frac{\mathrm{d}H_\nu}{\mathrm{d}z} = \eta_\nu - \chi_\nu J_\nu,$$

whereas for spherically symmetric, stationary, and (quasi-)static conditions, it reads

$$\frac{1}{r^2}\frac{\partial(r^2 H_\nu)}{\partial r} = \eta_\nu - \chi_\nu J_\nu. \tag{5.10}$$

We stress that the two preceding equations are valid only in case of *(quasi-)static* atmospheres, since otherwise the opacities become angle dependent, due to the apparent Doppler shifts (see Section 5.4), and cannot be put in front of the angular integrals. Thus, the latter two equations cannot be used in case of stellar winds, and the more general formulation of the RHS of (5.9) has to be accounted for. In an approximate way, though, these equations might still be applied for pure continuum problems in the presence of velocity fields, if an exact treatment of ionization edges plays a minor role.

The general first-order-moment equation is given by

$$\frac{1}{c^2}\frac{\partial}{\partial t}\mathcal{F}_\nu + \nabla \cdot \mathbf{P}_\nu = \frac{1}{c}\oint (\eta_\nu - \chi_\nu I_\nu)\,\mathbf{n}\mathrm{d}\Omega, \tag{5.11}$$

where now the frequency-integrated RHS is just the negative of the total radiation force, $-\mathbf{f}_{\mathrm{rad}} = -\rho \mathbf{g}_{\mathrm{rad}}$ (force exerted by radiation field onto the material).

The limit for plane-parallel, stationary and static conditions reads

$$\frac{\mathrm{d}K_\nu}{\mathrm{d}z} = -\chi_\nu H_\nu,$$

while for spherically symmetric, stationary and (quasi-)static conditions we find

$$\frac{\partial K_\nu}{\partial r} + \frac{3K_\nu - J_\nu}{r} = -\chi_\nu H_\nu. \tag{5.12}$$

The same caveats concerning (quasi-)static conditions as such as the preceding apply also here. We note as well that for static conditions the emissivity contribution to the radiation force vanishes, if the emission is isotropic as assumed here (since there are no Doppler shifts in this case).

5.3.2 *Solution Methods*

Ray-by-ray solution – p-z geometry. The following elegant method (based on Hummer and Rybicki, 1971) to solve the RTE for spherical atmospheres can be *only* applied to spherically symmetric problems, and for conditions where Doppler shifts do not play a decisive role, i.e., where opacities and emissivities can be assumed as isotropic (e.g., continuum formation in winds, if interactions of edges with other processes do not play a role). In brief, the methods works as follows (compare with Figure 5.5):

- Define p-rays (with impact parameter p) tangential to each discrete radial shell.
- Augment those with a bunch of (equidistant) p-rays resolving the core.

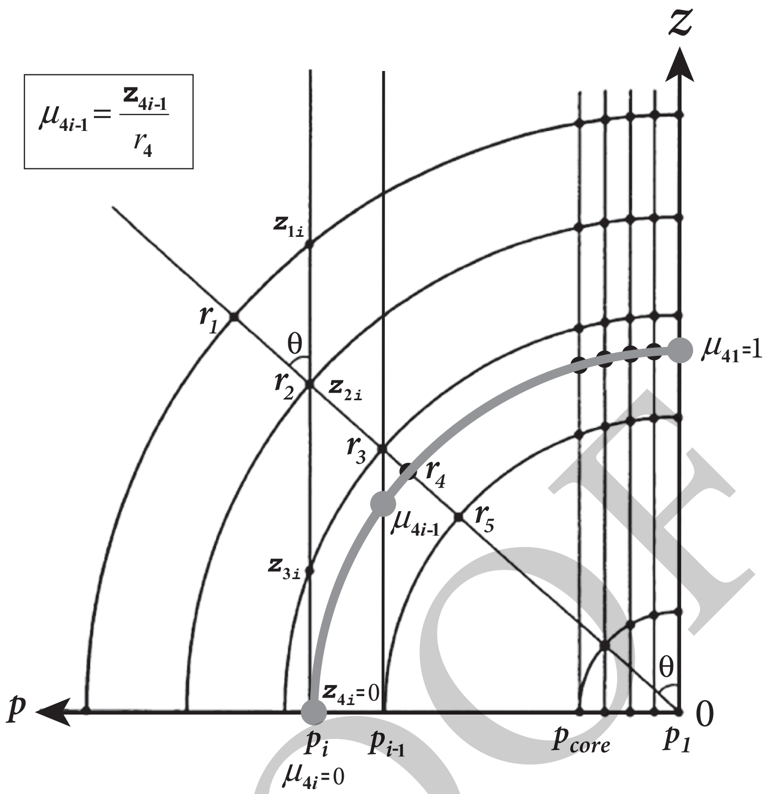

FIGURE 5.5. Sketch of p-z geometry (adapted from Mihalas, 1978). See text.

- Use only the forward hemisphere, i.e.,

$$z_{di} = \sqrt{r_d^2 - p_i^2} \quad \text{with} \quad z_{di} \geq 0.$$

  In this way, all points $z_{di}, i = 1, \mathrm{NP}$, are located on the same r_d-shell, i.e., have the same physical parameters, in particular emissivities and opacities (due to spherical symmetry and neglect of Doppler shifts).

Now one solves the RTE along each p-ray. From first principles,

$$\pm\frac{\mathrm{d}I_\nu^\pm(z,p_i)}{\mathrm{d}z} = \eta_\nu(r) - \chi_\nu(r) I_\nu^\pm(z,p_i)$$

with + for $\mu > 0$ and − for $\mu < 0$, using appropriate boundary conditions (core vs. noncore rays) and standard methods (finite differences, etc.). After being calculated, $I_\nu^\pm(z_{di}(r_d), p_i), i = 1, \mathrm{NP}$, samples the specific intensity at the same radius, r_d, but at different angles,

$$\pm\mu_{di} = \frac{z_{di}}{r_d},$$

starting at $|\mu_{di}| = 1$ for $i = 1$ and $d = 1, \mathrm{NZ}$ (central ray, $p_i = 0$) until $\mu_{di} = 0$ (tangent ray, where $p_i = r_d$ and thus $z_{di} = 0$). In other words, along individual r_d-shells, the specific intensities $I_\nu^\pm(r_d, \mu) = I_\nu^\pm(z_d, \mu)$ are sampled for all relevant μ, and corresponding moments can be calculated by integration.

Feautrier variables. In fact, the RTE is not solved for $I_\nu^\pm$ separately, but for a linear combination of I_ν^+ and I_ν^-, using the so-called Feautrier variables, u_ν and v_ν, which allows to construct a second-order scheme (higher accuracy, diffusion limit for large optical depths can be easily represented), similar as in the plane-parallel case:

$$u_\nu(z,p) = \frac{1}{2}(I_\nu^+(z,p) + I_\nu^-(z,p)) \qquad \text{mean intensity like}$$

$$v_\nu(z,p) = \frac{1}{2}(I_\nu^+(z,p) - I_\nu^-(z,p)) \qquad \text{flux like}$$

$$\Rightarrow \frac{\partial v_\nu}{\partial z} = \chi_\nu(S_\nu - u_\nu), \qquad \frac{\partial u_\nu}{\partial z} = -\chi_\nu v_\nu$$

$$\Rightarrow \frac{\partial^2 u_\nu}{\partial \tau_\nu^2} = u_\nu - S_\nu \qquad \text{(2nd order, with } \mathrm{d}\tau_\nu = -\chi_\nu \mathrm{d}z)$$

The source function S_ν is defined in the customary way as η_ν/χ_ν. Corresponding boundary conditions have to be provided, of course. For the inner boundary and for core rays, mostly a first-order condition using the diffusion approximation is applied, while for noncore rays, a second-order condition is formulated, using symmetry arguments. For the outer boundary, either $I_\nu^-(z_{\max}, p) = 0$ is set, or higher-order terms need to be accounted for, in case of optically thick conditions (e.g., at and bluewards of the He II edge). For atmospheres illuminated by companions, etc., this needs to be adapted.

As it turns out, this *formal solution* for $I_\nu(\mu)$ (or $u_\nu(\mu)$ and $v_\nu(\mu)$) and corresponding angle-averaged quantities (moments) is (partly strongly) affected by inaccuracies, due to the specific way of discretization within the p-z grid. However, the *ratios* of such moments (= Eddington factors) remain much more precise, since the aforementioned errors cancel to a major part.

The variable Eddington factor method. Thus, the conventional method to solve the RTE in spherically symmetric atmospheres (again: no Doppler shifts!) is to consider the moments equations (only radius-dependent), and to use the Eddington factors from the (previously described) formal solution to close the relations. This procedure ensures high accuracy (because of direct solution for angle-averaged quantities and second-order scheme), while the Eddington factors (from the formal solution) quickly stabilize in the course of global iterations. One additional advantage of using the moments equations is that the optimum diagonal accelerated lambda operator (see Section 5.5.2) can be easily calculated in parallel with the solution (and without major computational effort). Using the zero-order and first-order moment of the RTE ((5.10) and (5.12)), and the conventional Eddington factor $f_\nu = K_\nu/J_\nu$, we obtain

$$\frac{\partial(r^2 H_\nu)}{\partial \tau_\nu} = r^2(J_\nu - S_\nu) \quad \text{and} \quad \frac{\partial(f_\nu J_\nu)}{\partial \tau_\nu} - \frac{(3f_\nu - 1)J_\nu}{\chi_\nu r} = H_\nu,$$

now with $\mathrm{d}\tau_\nu = -\chi_\nu \mathrm{d}r$. Introducing a sphericality factor q_ν via

$$\ln(r^2 q_\nu) = \int_{r_{\rm core}}^{r} \left[\frac{3f_\nu - 1}{r' f_\nu}\right] \mathrm{d}r' + \ln(r_{\rm core}^2), \tag{5.13}$$

the second equation becomes

$$\frac{\partial(f_\nu q_\nu r^2 J_\nu)}{\partial \tau_\nu} = q_\nu r^2 H_\nu,$$

and can be combined with the first one to yield a second-order scheme for $r^2 J_\nu$,

$$\frac{\partial^2(f_\nu q_\nu r^2 J_\nu)}{\partial X_\nu^2} = \frac{1}{q_\nu} r^2 (J_\nu - S_\nu), \qquad \text{with } \mathrm{d}X_\nu = q_\nu \mathrm{d}\tau_\nu.$$

For comparison, the corresponding equation in p-p symmetry is given by

$$\frac{\partial^2(f_\nu J_\nu)}{\partial \tau_\nu^2} = (J_\nu - S_\nu),$$

and is just the limit of the spherically symmetric case, for $q_\nu \to 1$ and $r^2 \to R_*^2$.

5.4 Line Transfer in (Rapidly) Expanding Atmospheres

The basic problem for *line* transfer in rapidly expanding (or accreting) atmospheres is the Doppler shift (discarded in Section 5.3) that affects both opacities and emissivities, giving rise to an intricate coupling of location, frequency and angle. As detailed later, a very high resolution in the radial grid ($\Delta v = \mathrm{O}(v_{\mathrm{th}}/3)$) is required when standard (observer's frame) RT methods are applied[3], with v_{th} the thermal speed of the considered ion. E.g., for $v_\infty = 2{,}000 \ \mathrm{km\,s^{-1}}$, and $v_{\mathrm{th}} = 8 \ \mathrm{km\,s^{-1}}$ (representative for CNO-elements in a hot star wind), this leads to ≈750 radial grid points[4].

In such cases, only the RTE for the specific intensity should be solved (maybe cast to 'Rybicki form' if a separation into scattering and thermal part is possible), while the use of the aforementioned variable Eddington factor method is prohibitive, since it does not account for Doppler shifts.

In the following, we mostly consider the pure line case (except when stated differently), assuming that the continuum is optically thin (which is not so wrong for 'normal' OB-star winds, but invalid, e.g., for WR-star winds with much larger mass-loss rates).

Moreover, we assume pure Doppler broadening, which captures the essential broadening effect when calculating NLTE occupation numbers, etc., by means of scattering integrals, $\bar{J}$ (see (5.15)). For the calculation of emergent profiles, however, other broadening functions that describe also the line wings in a realistic manner (e.g., Stark and Voigt profiles) should be used if necessary.

5.4.1 *Notation: Line Opacity and Profile Function*

The inclusion of Doppler shifts leads to complications and possible confusion. Thus, before tackling the actual problem, we must define the notation we are going to use[5].

The line opacity, as a function of radial distance r and frequency ν, can be expressed as

$$\chi_\nu(r) = \bar{\chi}_{\mathrm{L}}(r)\phi(\nu, r)\ , \text{ with } \ \phi(\nu, r) = \frac{1}{\Delta\nu_{\mathrm{D}}(r)\sqrt{\pi}} \exp\left[-\left(\frac{\nu - \tilde{\nu}}{\Delta\nu_{\mathrm{D}}(r)}\right)^2\right]$$

$$\text{and} \quad \Delta\nu_{\mathrm{D}}(r) = \frac{\tilde{\nu} v_{\mathrm{th}}(r)}{c} \text{ for a Doppler profile.}$$

Here the profile function $\phi(\nu, r)$ is normalized with respect to frequency, and has dimensions $[\phi] = T$; $\tilde{\nu}$ is the line-center frequency, and v_{th} includes any kind of microturbulence (if present). The line opacity integrated over frequency is given by

[3] Many such methods also require a very high resolution in μ.

[4] This problem becomes mitigated when a large "microturbulence" of order 100 $\mathrm{km\,s^{-1}}$(due to an inhomogeneous wind structure) is accounted for (e.g., Hamann, 1980; Puls et al., 1993).

[5] Further specifications will be given in Appendix B.

$$\bar{\chi}_{\rm L}(r) = \frac{\pi e^2}{m_{\rm e} c}\, f_{lu} \left(n_l - n_u \frac{g_l}{g_u}\right),$$

where l and u denote the lower and upper levels of the transition, f_{lu} the oscillator strength, n_l and n_u the occupation numbers of the levels, and g_l and g_u the corresponding statistical weights. We stress that $[\bar{\chi}_L] = L^{-1}T^{-1}$, while $[\chi_\nu] = L^{-1}$.

When the material in the atmosphere is in motion with respect to the frame of an external observer at rest, matter particles "see" the radiation field at frequencies corresponding to their own *comoving frame* (CMF), and opacity and emissivity become *angle dependent* in the observer's frame, due to Doppler shifts. In fact, the atoms absorb and emit photons at frequency

$$\nu_{\rm CMF} = \nu - (\tilde{\nu}/c)\ \mathbf{n} \cdot \mathbf{v}(\mathbf{r}),$$

where ν is the frequency in the observer's frame, and nonrelativistic velocities are assumed. In spherical geometry, it holds that $\mathbf{n} \cdot \mathbf{v}(\mathbf{r}) = \mu v(r)$. The profile function, evaluated at CMF frequencies, is then

$$\phi(\nu_{\rm CMF}, r) = \frac{1}{\Delta\nu_{\rm D}(r)\sqrt{\pi}} \exp\left[-\left(\frac{\nu - \tilde{\nu} - \mu\, \tilde{\nu}\, v(r)/c}{\Delta\nu_{\rm D}(r)}\right)^2\right].$$

For simplicity's sake, in the following we will assume that $v_{\rm th}$ is spatially constant[6] and define, in the observer's frame, the frequency shift measured in Doppler units as

$$x \equiv \frac{\nu - \tilde{\nu}}{\Delta\nu_{\rm D}} \quad \text{with} \quad \Delta\nu_{\rm D} = \frac{\tilde{\nu} v_{\rm th}}{c}.$$

With the preceding choice, the transformation between observer's frame and CMF is

$$x_{\rm CMF} = x - \mu v'(r), \quad \text{with} \quad v'(r) = \frac{v(r)}{v_{\rm th}} \quad \in \left(0, \frac{v_\infty}{v_{\rm th}} >> 1\right),$$

so that

$$\phi_\nu(x_{\rm CMF}, r) = \phi_\nu(x - \mu v', r) = \frac{1}{\Delta\nu_{\rm D}\sqrt{\pi}} \exp\left[-\left(x - \mu v'(r)\right)^2\right],$$

The preceding profile function, whose dimension is still T, depends primarily on $x_{\rm CMF}$.

In order to simplify the following discussion, it is convenient to include the factor $(\Delta\nu_{\rm D})^{-1}$ into the opacity, so that the profile function, in units of Doppler shift, is now dimensionless (and normalized with respect to x), whilst $[\bar{\chi}_{\rm L}(r)/\Delta\nu_{\rm D}] = L^{-1}$. We then have

$$\chi_\nu(x_{\rm CMF}, r) = \frac{\bar{\chi}_{\rm L}(r)}{\Delta\nu_{\rm D}} \phi(x_{\rm CMF}, r)\ , \text{ with } \ \phi(x_{\rm CMF}, r) = \frac{1}{\sqrt{\pi}} \exp\left[-\left(x - \mu v'(r)\right)^2\right],$$

$$\text{and} \quad \frac{\bar{\chi}_{\rm L}(r)}{\Delta\nu_{\rm D}} = \frac{\bar{\chi}_{\rm L}(r)\tilde{\lambda}}{v_{\rm th}}.$$

Since $\mu v'(r) \in [-v_\infty/v_{\rm th}], +v_\infty/v_{\rm th}]$, x must vary within the same range (essentially, $x \in [-\infty, +\infty]$), and not only within a range of a few thermal Doppler widths[7].

[6] The generalization to a depth-dependent $v_{\rm th}$ will be considered in Appendix B.1.
[7] Several integrals involving $\phi(x)$ are presented in Appendix B.2.

5.4.2 *Sobolev Theory*

The resonance zone. Since $\mu v'(r)$ enters into the argument of ϕ, we must know (for instance, for computing the optical depth) the variation of the former quantity along a path ds, i.e., $\mathrm{d}\mu v'(r)/\mathrm{d}s$. (Recall that $\mathbf{n}\cdot\nabla = \mathrm{d}/\mathrm{d}s$.) We consider again a $p-z$ geometry, in which the z-axis shall be parallel to $\mathbf{n}$, and obtain

$$\frac{\mathrm{d}\mu v'(r)}{\mathrm{d}s} \rightarrow \left.\frac{\mathrm{d}\mu v'(r)}{\mathrm{d}z}\right|_p = \mu \left.\frac{\mathrm{d}v'}{\mathrm{d}r}\frac{\mathrm{d}r}{\mathrm{d}z}\right|_p + \left.\frac{\mathrm{d}\mu}{\mathrm{d}z}\right|_p v' = \mu^2\frac{\mathrm{d}v'}{\mathrm{d}r} + (1-\mu^2)\frac{v'}{r}.$$

Note that contrasted to Section 5.3.2, $\mu < 0$ implies here that $z < 0$, so that for negative angles we consider the back hemisphere of the $p-z$ system. Moreover it holds that

$$\mu^2\frac{\mathrm{d}v'}{\mathrm{d}r} + (1-\mu^2)\frac{v'}{r} > 0 \quad \text{for} \quad v' > 0 \quad \text{and} \quad \frac{\mathrm{d}v'}{\mathrm{d}r} > 0.$$

Thus, in spherical symmetry $\mu v'(r)$ increases monotonically along *any* given direction $\mathbf{n}$, as long as $v'(r) > 0$ is monotonically increasing.

Now, as the optical depth is defined by

$$\tau_x(z) = \int_{z_{\min}}^{z} \frac{\bar{\chi}_{\mathrm{L}}(z')}{\Delta\nu_{\mathrm{D}}}\phi\left(x - [\mu v'](z'), z'\right)\mathrm{d}z',$$

it depends on the argument of the profile function, and it is clear that line processes are only effective in a (very) localized region, the so-called *resonance zone*, whenever $\phi(x_{\mathrm{CMF}})$ is nonnegligible, i.e., when $(x - \mu v') \in [-\Delta x_{\mathrm{Dop}}, +\Delta x_{\mathrm{Dop}}] \approx [-3, 3]$ (see Figure 5.6).

In order to achieve a proper representation of the line transfer process, both frequencies x and projected velocities $\mu v'(z)$ must be highly resolved, on scales corresponding to v_{Dop}. If, on the one hand, the $\mu v'(z)$-spacing were too coarse, the resonance zones would be missed or not resolved, the intensities would remain constant (or too large), and the quantity $\bar{I}$ (related to the scattering integral, and required later on; see Figure 5.6) would become too large. With regard to Figure 5.6, this would mean that in the most extreme case, all three curves (intensities) would remain constant, at a value equal to I_0, resulting in a dramatic overestimate of $\bar{I}$. If, on the other hand, the x-spacing was too coarse, the variation of $I(x)$ (from 'neighboring' resonance zones) would be insufficiently sampled. For our example, this could mean that the left and/or right curves were absent (due to missing frequencies), and the middle curve would not be centered, since there might be no frequency where $x - \mu v'$ is *exactly* zero.

In spherical geometry, the first point is a specific problem, since the general spacing refers to the radial grid (and not to specific p-rays), and a high resolution in $v'(r)$ does not guarantee a high resolution in $\mu v'(z)$. In models using cartesian coordinates (μ=const along a specific ray), the first point leads to the condition that $\Delta\mu = \Delta x/v'_{\max}$, i.e., an intricate coupling of frequency and angle.

'Standard' Sobolev theory. As discussed in the previous paragraph, line processes (contrasted to continuum ones) occur in a very localized region within a rapidly expanding medium. V. Sobolev (1960; but work done already during World War II) was the first to obtain a completely local approximation that is quite accurate (and can be extended to become even more precise). The following reasoning follows (in part) Owocki and Puls (1996); for an alternative and very insightful derivation, see Rybicki and Hummer (1978). For simplicity, in this reasoning, we do the following:

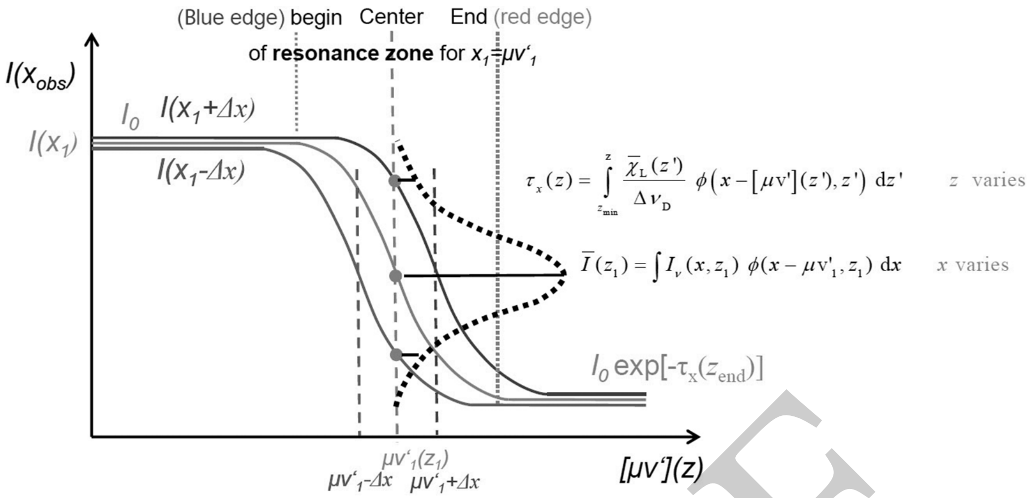

FIGURE 5.6. Radiative line transfer in expanding atmospheres: resonance zones and related aspects, for the case of pure absorption. Displayed is the specific intensity along an arbitrary ray, as a function of $[\mu v'](z) = \mu(z)v'(r(z))$ ($v' > 0$ for outflows). The three curves show the variation of the intensity when crossing the corresponding resonance zones, for observer's frame frequencies x_1 (central curve), $x_1 + \Delta x$ (rightmost curve), and $x_1 - \Delta x$ (leftmost curve), respectively. The centers of the resonance zones are marked by dashed vertical lines. The evaluation of the quantity $\bar{I}(z_1)$ (see insert) is indicated as well. For this quantity, the intensities from different frequencies contribute as follows: at the considered location z_1, $I(x_1 + \Delta x)$ (rightmost curve) has just entered its own resonance zone, $I(x_1)$ needs to be evaluated at the center of the resonance zone corresponding to $\mu v'(z_1) = x_1$, and $I(x_1 - \Delta x)$ (leftmost curve) has almost passed its resonance zone. Obviously, the largest contribution is provided by $I(x_1, z_1)$. Note the intricate coupling between location and frequency.

- Concentrate on outflows, i.e., $v(r) > 0$ (but $\mathrm{d}v/\mathrm{d}r < 0$, as occurring, e.g., in flows with embedded shocks, is not excluded).
- Adopt, as before, a spatially constant thermal speed, $v_{\rm th}(r) := v_{\rm th}$
- Define $\chi_1(r) = \bar{\chi}_{\rm L}(r)/\Delta\nu_{\rm D}$.

Under such conditions, the optical depth difference between two points z_1 and z_2 (along impact parameter p) is given by

$$t(x, p, z_1, z_2,) = \int_{\min(z_1,z_2)}^{\max(z_1,z_2)} \chi_1(r')\,\phi(x - \mu' v'(r'))\,\mathrm{d}z' \tag{5.14}$$

with (as usual) $\mu' = z'/r'$, and $r' = \sqrt{z'^2 + p^2}$. Then, without any approximation,

$$I_\nu(x, p, z)$$

$$= \underbrace{I_{\rm core}\,\mathrm{e}^{-t(x,p,z,z_B)}}_{\substack{\text{direct component, only present}\\ \text{for } \mu>0 \text{ and } p\le R_*}} + \underbrace{\int_0^{t(x,p,z,z_B)} S(r')\mathrm{e}^{-t(x,p,z,z')}\mathrm{d}t(x,p,z,z')}_{\text{diffuse component (radiation scattered/emitted in the wind)}}$$

with

$$z_B = \begin{cases} z_* \text{ for } z > 0,\ p \le R_* \\ -\infty \text{ else} \end{cases}$$

This equation is valid for both outwards ($\mu \geq 0$) and inwards ($\mu < 0$) rays, depending on the sign of z. (Here, we use a p-z geometry extending over both hemispheres, with $z > 0$ for the front, and $z < 0$ for the back hemisphere.)

To calculate the scattering integrals, required to couple with the rate equations, we first integrate over $\phi(x)\mathrm{d}x$,

$$\bar{I}(\mu, r) = \int_{-\infty}^{+\infty} I_\nu(x, \mu, r)\phi\left(x - \mu v'(r)\right)\mathrm{d}x, \qquad \text{and then over } \mathrm{d}\mu,$$
$$\bar{J}(r) = \frac{1}{2}\int_{-1}^{+1} \bar{I}(\mu, r)\ \mathrm{d}\mu \tag{5.15}$$

Now we consider that the integrands provide a contribution only if $x \approx \mu' v'(r')$ (5.14) or $x \approx \mu v'(r)$ (5.15), respectively, due to the behaviour of ϕ. For the optical depth difference, this means that

$$t(x, p, z, z_B,) = \int_{\min(z,z_B)}^{\max(z,z_B)} \chi_\mathrm{l}(r')\phi\left(x - \mu' v'(r')\right)\mathrm{d}z' \approx \chi_\mathrm{l}(r_0)\int_{\mathrm{z_{min}}}^{\mathrm{z_{max}}} \phi\left(x - \mu' v'(r')\right)\mathrm{d}z', \tag{5.16}$$

where r_0 is the position of the corresponding resonance zone, which (at least in principle) needs to be calculated from

$$\left[\mu' v'\right](r_0) = x, \qquad \text{i.e., } \pm\sqrt{1 - \frac{p^2}{r_0^2}}v'(r_0) = x \qquad \text{(nonlinear eq.)},$$

which has a unique solution for strictly monotonic flows (otherwise there is more than one resonance zone). The RHS of (5.16) constitutes the heart of the *Sobolev approximation*: line opacities (and source functions, discussed later in this section) are assumed to be constant over the resonance zones!

Furthermore, we switch from an integration over $\mathrm{d}z'$ to an integration over CMF frequency, $\mathrm{d}x_\mathrm{CMF} = \mathrm{d}(x - \mu' v'(r'))$,

$$\left.\frac{\mathrm{d}x_\mathrm{CMF}}{\mathrm{d}z}\right|_p = -\left.\frac{\mathrm{d}(\mu v')}{\mathrm{d}z}\right|_p = \text{(see Section 5.4.2)} = -\left(\mu^2\frac{\mathrm{d}v'}{\mathrm{d}r} + (1-\mu^2)\frac{v'}{r}\right) =: -Q(r, \mu).$$

For $Q > 0$, we have the following situation: by considering the boundaries, $x_\mathrm{CMF}(z) = x - \mu v'(r)$, $x_\mathrm{CMF}(z_B) \to \infty$ (bluewards of blue edge of resonance zone), and by putting $Q(r', \mu')$ in front of the integral (using the same argument as before), we arrive at

$$t(x, p, z, z_B) \approx \chi_\mathrm{l}(r_0)\int_{x_\mathrm{CMF}(\mathrm{z_B})}^{x_\mathrm{CMF}(\mathrm{z})} \frac{-1}{Q(r', \mu')}\,\phi(x_\mathrm{CMF})\,\mathrm{d}x_\mathrm{CMF} \approx$$
$$\approx \frac{\chi_\mathrm{l}(r_0)}{Q(r_0, \mu_0)}\int_{x - \mu v'(z)}^{\infty} \phi(\xi)\ \mathrm{d}\xi = \tau_\mathrm{S}(r_0, \mu_0)\ \Phi(x - \mu v'(r)) \tag{5.17}$$

This result can be generalized to also include negative values of Q, if we define

$$\tau_S(r_0, \mu_0) = \frac{\chi_\mathrm{l}(r_0)}{|Q(r_0, \mu_0)|} = \frac{\bar{\chi}_\mathrm{L}(r_0)}{\Delta\nu_\mathrm{D}\left|\mu^2\frac{\mathrm{d}v'}{\mathrm{d}r} + (1-\mu^2)\frac{v'}{r}\right|_{r_0,\mu_0}} \tag{5.18}$$

as the Sobolev optical depth, evaluated at the resonance zone. In the most general case, Q is the directional derivative of the velocity in direction $\mathbf{n}$, i.e.,

$$|Q| = |\mathbf{n} \cdot \nabla(\mathbf{n} \cdot \mathbf{v}')| = \left|\frac{\mathrm{d}v'_l}{\mathrm{d}l}\right|, \text{ if } l \text{ has direction } \mathbf{n}.$$

For a further understanding of Equations (5.17) and (5.18), a few comments might be relevant:

- $\Phi(\infty) = 0$ (blue – starwards – side of resonance zone), and $\Phi(-\infty) = 1$ (red side of resonance zone), as long as $v > 0$. Thus:
  $t(x, p, z, z_B) \to 0$ for z 'before' the resonance zone, and $I(z) = I_{\mathrm{core}}$.
  $t(x, p, z, z_B) \to \tau_S$ for z 'behind' the resonance zone, and $I(z) \approx I_{\mathrm{core}} \exp(-\tau_{\mathrm{S}})$ (without emission, compare with Figure 5.6).
- For pure Doppler-profiles, $\Phi(x) = \frac{1}{2}\mathrm{erfc}(x)$.
- Since v' is the velocity in units of the thermal speed, and since $\Delta\nu_{\mathrm{D}} = v_{\mathrm{th}}/\tilde{\lambda}$, we can alternatively write

$$\tau_S(r_0, \mu_0) = \frac{\bar{\chi}_{\mathrm{L}}(r_0)\,\tilde{\lambda}}{\left|\mu^2 \frac{\mathrm{d}v}{\mathrm{d}r} + (1-\mu^2)\frac{v}{r}\right|_{r_0,\mu_0}},$$

  when v and r are measured in actual units (then v/r has units of s^{-1}).

Since also the integrand of the diffuse component contributes only for $x \approx \mu' v'$,

$$\int\limits_0^{t(x,p,z,z_B)} S(r')\,\mathrm{e}^{-t(x,p,z,z')}\,\mathrm{d}t(x,p,z,z') \to S(r_0)\int\limits_0^{t} \mathrm{e}^{-t'}\mathrm{d}t' = S(r_0)\left(1-\mathrm{e}^{-t}\right),$$

the specific intensity can be approximated by

$$I_\nu(x,p,z) \approx I_{\mathrm{core}}(p)\mathrm{e}^{-\tau_{\mathrm{S}}(r_0,\mu_0)\Phi(x_{\mathrm{CMF}})} + S(r_0)\left(1-\mathrm{e}^{-\tau_{\mathrm{S}}(r_0,\mu_0)\Phi(x_{\mathrm{CMF}})}\right). \tag{5.19}$$

This means that behind the resonance zone (where $\Phi(x_{\mathrm{CMF}}) = 1$),

$$I_\nu(x,p,z_{\mathrm{behind}}) \approx I_{\mathrm{core}}(p)\mathrm{e}^{-\tau_{\mathrm{S}}(r_0,\mu_0)} + S(r_0)\left(1-\mathrm{e}^{-\tau_{\mathrm{S}}(r_0,\mu_0)}\right) = \text{const},$$

while before the resonance zone (where $\Phi(x_{\mathrm{CMF}}) = 0$),

$$I_\nu(x,p,z_{\mathrm{before}}) \approx \begin{cases} I_{\mathrm{core}}(p)\text{=const for } & p \le R_* \\ 0 \quad \text{else} \end{cases}$$

Only inside the resonance zone, the optical depth increases and the intensity varies accordingly (again, compare with Figure 5.6).

We stress that to calculate the *specific intensity* in Sobolev approximation (required, e.g., for the emergent profile), the location of the resonance zone has to be evaluated for each frequency and impact parameter!

Now comes the second 'trick'. As already outlined, we first calculate

$$\bar{I}(r,\mu) = \int\limits_{-\infty}^{+\infty}\left[I_{\mathrm{core}}(p)\mathrm{e}^{-\tau_{\mathrm{S}}(r_0,\mu_0)\Phi(x_{\mathrm{CMF}})} + S(r_0)\left(1-\mathrm{e}^{-\tau_{\mathrm{S}}(r_0,\mu_0)\Phi(x_{\mathrm{CMF}})}\right)\right]\phi(x_{\mathrm{CMF}}(r,\mu))\mathrm{d}x$$

Again, we find a contribution only for $x_{\rm CMF} \approx 0$, i.e., $x \approx \mu v'(r)$. Thus, we can replace r_0 by r and μ_0 by μ: only those frequencies/resonance zones contribute that are located at (or close to) the considered location (r, μ).

Realizing that $\phi(x_{\rm CMF}){\rm d}x = -{\rm d}\Phi$ with $\Phi(x_{\rm CMF} = x - \mu v') \to 1$ for $x \to -\infty$ and $\Phi(x_{\rm CMF} = x - \mu v') \to 0$ for $x \to \infty$, we find

$$\bar{I}(r,\mu) \approx \int\limits_0^1 \left[I_{\rm core}(p){\rm e}^{-\tau_{\rm S}(r,\mu)\Phi(x_{\rm CMF})} + S(r)\left(1 - {\rm e}^{-\tau_{\rm S}(r,\mu)\Phi(x_{\rm CMF})}\right)\right] {\rm d}\Phi =$$
$$= I_{\rm core}(p)\frac{1-{\rm e}^{-\tau_{\rm S}(r,\mu)}}{\tau_{\rm S}(r,\mu)} + S(r)\left(1 - \frac{1-{\rm e}^{-\tau_{\rm S}(r,\mu)}}{\tau_{\rm S}(r,\mu)}\right),$$

which is thus *purely local*. Finally, by integrating over ${\rm d}\mu$, and accounting for the limits regarding the first term,

$$\begin{aligned} \bar{J}(r) &= \beta_{\rm c}(r) I_{\rm core} + (1-\beta(r))\,S(r), && \text{with} \\ \beta_{\rm c}(r)I_{\rm core} &= \frac{1}{2}\int\limits_{\mu_*}^1 I_{\rm core}(\mu,\bar{\nu})\frac{1-{\rm e}^{-\tau_{\rm S}(r,\mu)}}{\tau_{\rm S}(r,\mu)}{\rm d}\mu, && \text{and} \\ \beta(r) &= \frac{1}{2}\int\limits_{-1}^1 \frac{1-{\rm e}^{-\tau_{\rm S}(r,\mu)}}{\tau_{\rm S}(r,\mu)}{\rm d}\mu && \text{(escape probability).} \end{aligned} \tag{5.20}$$

We note the following:

(i) The angular integration does *not* require a highly resolved angular grid, since the interaction between x, μ and r has already been accounted for.

(ii) The core intensity has to be emitted (evaluated) at the core for an observer's (rest) frame frequency of $\bar{\nu} \approx \tilde{\nu}\,(1 + \mu v(r)/c)$, in order to display a local CMF-frequency of $\nu_{\rm CMF} \approx \tilde{\nu}$ at $[\mu v(r)]$, corresponding to a local $x_{\rm CMF} = 0$. This ensures that the resonance zone is illuminated by the full core intensity, and that there are no self-shadowing effects (at least if there are no line-overlap effects).

Sobolev optical depth for prototypical resonance lines. The Sobolev optical depth at (r, μ),

$$\tau_S(r,\mu) = \frac{\chi_{\rm l}(r)}{|Q(r,\mu)|} = \frac{\bar{\chi}_{\rm L}(r)}{\Delta\nu_{\rm D}\left|\mu^2\frac{{\rm d}v'}{{\rm d}r} + (1-\mu^2)\frac{v'}{r}\right|},$$

results for radial rays ($\mu = 1$) in

$$\tau_S(r) = \bar{\chi}_{\rm L}(r)\tilde{\lambda}/|{\rm d}v/{\rm d}r|.$$

For ground-state opacities of main ionization stages as present in many UV resonance lines, we have $\bar{\chi}_{\rm L}(r) \propto n_1(r) \propto \rho(r)$, and, exploiting the continuity equation, $\rho(r) = \dot{M}/(4\pi r^2 v(r))$, and the typical β-velocity law, we obtain

$$\tau_S(r) \propto \frac{1}{r^2\ v(r)\ \frac{{\rm d}v}{{\rm d}r}} = \frac{1}{\beta b R_* v_\infty^2}\left(\frac{v(r)}{v_\infty}\right)^{\frac{1}{\beta}-2},$$

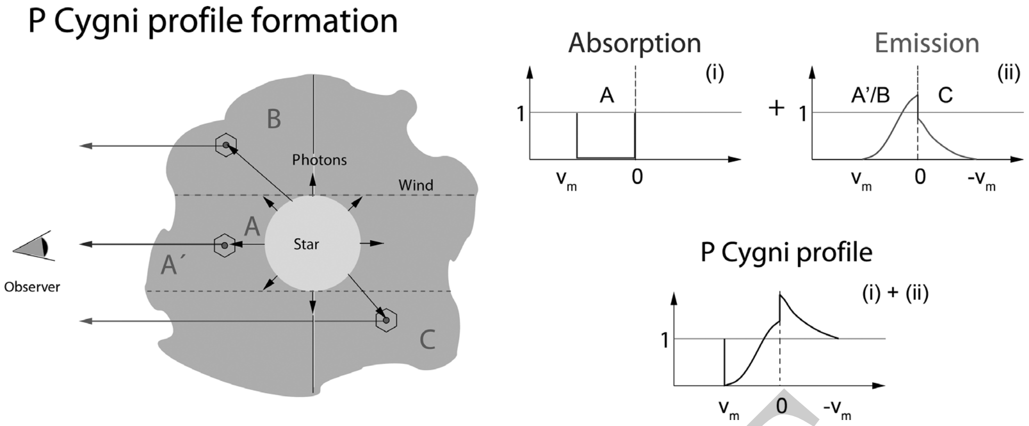

FIGURE 5.7. Principle of P Cygni-profile formation, for a strong resonance line, remaining optically thick until a maximum velocity, v_m. Due to Doppler shifts, all observer's frame frequencies corresponding to $[+v_m, -v_m]$ can contribute. (i) Absorption in region A in front of the stellar disk (approaching material → blue frequencies). (ii) Asymmetric emission from regions A/B in front hemisphere (blue emission due to approaching material), and region C (side lobes) in back hemisphere (red emission due to receding material). The emission itself is caused by line scattering; see the leftmost sketch.

with $b = 1 - (v_{\min}/v_\infty)^{1/\beta}$. For $\beta = 0.5$[8], this implies $\tau_S(r) = $ const, while for a more typical situation with $\beta = 1$, $\tau_S(r) \propto v_\infty/v(r)$, and the optical depth decreases by roughly (and only) a factor of 100 from inside to outside. This explains why a typical UV P Cygni line, e.g., C IV 1548/1550 (Figure 5.1), remains optically thick throughout the *complete* wind, displaying a saturated absorption trough even for frequencies corresponding to v_∞ (see also Figure 5.7).

Limiting cases: source functions for purely scattering resonance lines. Very often, the source functions of the aforementioned resonance lines are dominated by line-scattering, and in such cases (see also Section 5.5),

$$S(r) = \bar{J}(r) = \frac{\beta_{\mathrm{c}}(r) I_{\mathrm{core}}}{\beta(r)}.$$

(a) In the optically thin limit, i.e., (locally) weak resonance lines, $\tau_S(r,\mu) \ll 1$,

$$\frac{1 - e^{-\tau_S(r,\mu)}}{\tau_S(r,\mu)} \to 1, \quad \text{and} \quad S(r) = \frac{\beta_{\mathrm{c}}(r) I_{\mathrm{core}}}{\beta(r)} \to W I_{\mathrm{core}},$$

with dilution factor W (5.7). Thus, for large distances from the stellar core,

$$\left(\frac{r}{R_*}\right)^2 S(r) \to \frac{I_{\mathrm{core}}}{4} = \text{const},$$

and the source function dilutes quadratically. This can be also understood in terms of an alternative argumentation: For an optically thin line, $\bar{J} \approx J_\nu$, and for an optically thin continuum as assumed here $J_\nu \to W I_{\mathrm{core}}$ (see Section 5.3.1). Since $S = \bar{J}$, we thus have $S = W I_{\mathrm{core}}$.

[8] This corresponds to a velocity field in line-driven winds when neglecting the so-called finite cone-angle correction factor, e.g., Castor et al. (1975).

(b) In the optically thick limit, $\tau_S(r,\mu) \gg 1$, which applies to strong UV resonance lines (discussed previously),

$$\frac{1-e^{-\tau_S(r,\mu)}}{\tau_S(r,\mu)} \to \frac{1}{\tau_S(r,\mu)},$$

and (after few calculations),

$$S(r) = \frac{\beta_\mathrm{c}(r) I_\mathrm{core}}{\beta(r)} \to \left(\frac{R_*}{r}\right)^2 I_\mathrm{core} \frac{3}{4+8\left(\frac{\mathrm{d}\ln v}{\mathrm{d}\ln r}\right)^{-1}} \quad \text{for large radii.}$$

Since for large radii and a β velocity law $\mathrm{d}\ln v/\mathrm{d}\ln r \propto R_*/r$, the source function of an optically thick resonance line becomes proportional to $(R_*/r)^3$, and *decreases faster* than in the optically thin case. Also, this behaviour is important to understand the absorption troughs of UV P Cygni lines at high velocities.

Radiative line acceleration. In Sobolev approximation, the radiative line acceleration due to *one* line is provided by[9]

$$g_\mathrm{rad} = \frac{4\pi}{c}\frac{\bar{\chi}_\mathrm{L}}{\rho}\frac{1}{2}\int \bar{I}(\mu)\mu\mathrm{d}\mu \approx \frac{2\pi}{c}\frac{\bar{\chi}_\mathrm{L}}{\rho}\int_{\mu_*}^{1} I_\mathrm{core}(\mu,\bar{\nu})\frac{1-\mathrm{e}^{-\tau_\mathrm{S}(r,\mu)}}{\tau_\mathrm{S}(r,\mu)}\mu\mathrm{d}\mu,$$

since the contribution from the source term (even in μ) cancels when integrating over $\mu\mathrm{d}\mu$ with $\mu \in [-1,1]$. In particular,

$$g_\mathrm{rad} \propto \frac{\bar{\chi}_\mathrm{L}}{\rho}, \qquad \text{and NOT} \quad \propto \frac{\bar{\chi}_\mathrm{L}}{\rho\Delta\nu_D} \qquad \text{(see Appendix B.2).}$$

In the optically thick case, $\tau_\mathrm{S} = \bar{\chi}_\mathrm{L}/(\Delta\nu_D\,|Q(r,\mu)|) \gg 1$,

$$g_\mathrm{rad} \stackrel{\tau_\mathrm{S}\gg 1}{\to} \frac{2\pi}{c}\frac{\bar{\chi}_\mathrm{L}}{\rho}\frac{1}{\bar{\chi}_\mathrm{L}/\Delta\nu_D}\int_{\mu_*}^{1} I_\mathrm{core}(\mu,\bar{\nu})\,|Q(r,\mu)|\,\mu\mathrm{d}\mu,$$

and the line acceleration becomes independent of $\bar{\chi}_\mathrm{L}$

$$g_\mathrm{rad} \stackrel{\tau_\mathrm{S}\gg 1}{\to} \frac{2\pi\Delta\nu_D}{c\rho}\int_{\mu_*}^{1} I_\mathrm{core}(\mu,\bar{\nu})\,|Q(r,\mu)|\;\mu\,\mathrm{d}\mu,$$

with $|Q(r,\mu)| = \left|\mu^2\mathrm{d}v'/\mathrm{d}r + (1-\mu^2)v'/r\right|$.

Sobolev length. The Sobolev length is roughly the (half-)width of the resonance zone. More precisely, it is the length scale on which $v(r)$ changes by one v_th unit, accounting for the most decisive part of the line profile:

$$\Delta v = v_\mathrm{th} := \left|\frac{\mathrm{d}v}{\mathrm{d}r}\right| L_\mathrm{Sob} \quad \Rightarrow \quad L_\mathrm{Sob} = \frac{v_\mathrm{th}}{|\mathrm{d}v/\mathrm{d}r|} = \frac{1}{|\mathrm{d}v'/\mathrm{d}r|} \quad \text{for radial rays, and}$$

$$\Delta v = v_\mathrm{th} := \left|\frac{\mathrm{d}(\mu v)}{\mathrm{d}z}\right| L_\mathrm{Sob} \quad \Rightarrow \quad L_\mathrm{Sob} = \frac{v_\mathrm{th}}{\left|\mu^2\frac{\mathrm{d}v}{\mathrm{d}r} + (1-\mu^2)\frac{v}{r}\right|} = \frac{1}{\left|\mu^2\frac{\mathrm{d}v'}{\mathrm{d}r} + (1-\mu^2)\frac{v'}{r}\right|}$$

[9] Compare with (5.11), and account for the fact that *when integrated over frequency*, there is no force associated with emission, since there is no net momentum transfer due to an emission process presumed to be isotropic; see also Castor (1974).

for spherical symmetry. Most generally, the Sobolev length in direction $\mathbf{n}$ is

$$L_{\rm Sob} = \frac{v_{\rm th}}{|\mathbf{n} \cdot \nabla(\mathbf{n} \cdot \mathbf{v})|}$$

We note that for low microturbulent velocities, $L_{\rm Sob}$ depends on $m_{\rm ion}^{-1/2}$, i.e., decreases significantly from H to Fe.

Range of validity of the Sobolev approximation. Let's define a characteristic length scale, l_x, for a macrovariable x, defined via

$$\frac{\mathrm{d}x}{\mathrm{d}r} l_x = x, \quad \text{i.e.,} \quad l_x = \left(\frac{\mathrm{d}\ln x}{\mathrm{d}r}\right)^{-1}.$$

To warrant the validity of the Sobolev approximation (SA), $L_{\rm Sob}$ must be smaller than l_x,

$$\left|\frac{L_{\rm Sob}}{l_x}\right| = \left|\frac{\mathrm{d}\ln x}{\mathrm{d}v/v_{\rm th}}\right| < 1.$$

As an important example, we consider the (frequency-integrated) line opacity, assumed within the SA as being roughly constant over the resonance zone when evaluating the optical-depth integrals. For many (UV) resonance lines, $\bar{\chi}_{\rm L}(r) \propto \rho(r)$ (discussed previously), and a typical velocity field reads $v(r) = v_\infty(1 - \frac{R_*}{r})^\beta$, with $\beta \approx 1$, and neglecting the quantity $b \approx 1$ that plays no role here. Then,

$$\left|\frac{L_{\rm Sob}}{l_{\bar{\chi}_{\rm L}}}\right| = \frac{v_{\rm th}}{v} + \frac{2v_{\rm th}}{v_\infty}\frac{r}{R_*},$$

and the Sobolev approximation is valid (regarding an opacity $\propto \rho$) as long as the following are true:

(i) $v(r) > v_{\rm th}$ (sometimes, the SA is also called a supersonic approximation, though in view of this result it should be called superthermal).

(ii) $r/R_* < v_\infty/(2v_{\rm th}) = O(100)$, i.e., for all relevant radii.

As it turns out, a similar condition applies for the source function. The following are the only regions (in a smooth wind) where the SA inevitably fails:

- The subthermal region, where the density increases exponentially within a very extended resonance zone
- The transition zone between the quasihydrostatic photosphere and wind, where the resonance zone is still broad, but the velocity field has a significant curvature, and not a constant gradient[10].

Interestingly, the SA is almost perfectly valid in a supernova remnant, due to its homologous expansion, $v \propto r$, i.e., a constant gradient. However, when applied to line-driven winds, the SA fails in correctly describing the reaction of the line acceleration onto disturbances. Most important, the so-called line-driven instability (LDI) cannot be represented in the framework of the SA (e.g., Owocki and Rybicki, 1984).

5.4.3 *Extensions of the Sobolev Theory*

Particularly in the 1980s and 1990s, the 'standard' Sobolev theory (adopting an optically thin continuum and constant velocity gradients, line opacities and source functions over the resonance zone) has been extended towards more complex physical scenarios.

[10] Unfortunately, this zone is very important for the radiative line acceleration, and is badly described when using the SA (see Owocki and Puls, 1999).

Coupling with continuum. Hummer and Rybicki (1985) accounted for continua of arbitrary optical depth, and coupled the line with the continuum transfer. In this case,

$$\bar{J}(r) = \overline{\beta_{\mathrm{c}}(r) I_{\mathrm{inc}}} + (1 - \beta(r))\, S_{\mathrm{L}}(r) + (S_{\mathrm{c}}(r) - S_{\mathrm{L}}(r))\, \bar{U}(\tau_{\mathrm{S}}, \beta_{\mathrm{P}}),$$

$$\text{with} \qquad \overline{\beta_{\mathrm{c}}(r) I_{\mathrm{inc}}} = \frac{1}{2} \int_{-1}^{1} I^{\mathrm{inc}}(r, \mu) \frac{1 - \mathrm{e}^{-\tau_{\mathrm{S}}(r,\mu)}}{\tau_{\mathrm{S}}(r, \mu)} \mathrm{d}\mu, \tag{5.21}$$

and $I^{\mathrm{inc}}(r, \mu)$ the intensity incident to the considered location (resonance zone), usually the continuum intensity. In (5.21), $\beta(r)$ is the (conventional) escape probability[11], $S_{\mathrm{c}}(r)$ the continuum source function and $\bar{U}(\tau_{\mathrm{S}}, \beta_{\mathrm{P}})$ a function describing the actual coupling of the opacities in the resonance zone, with $\beta_{\mathrm{P}} = \frac{\chi_{\mathrm{c}}}{\bar{\chi}_{\mathrm{L}}/\Delta\nu_D}$ the ratio between continuum and line opacity. The function $\bar{U}$ can be obtained, e.g., from precalculated tables (Taresch et al., 1997).

Often the last term in (5.21) can be neglected, but at least the first term (modified compared to the previous expressions) needs to be considered when the continuum is nonnegligible. To evaluate this term, one either uses the intensities from the continuum transfer, or one applies the following reasoning (unpublished thus far):

$$\begin{aligned}
\overline{\beta_{\mathrm{c}}(r) I_{\mathrm{inc}}} &= \frac{1}{2} \int_{-1}^{1} I^{\mathrm{inc}}(r, \mu) \frac{1 - \mathrm{e}^{-\tau_{\mathrm{S}}(r,\mu)}}{\tau_{\mathrm{S}}(r, \mu)} \mathrm{d}\mu \\
&\overset{\tau_{\mathrm{S}} \gg 1, \mathrm{d}v/\mathrm{d}r > 0}{\rightarrow} \frac{1}{2\chi_l} \int_{-1}^{1} I^{\mathrm{inc}}(r, \mu) \left[\mu^2 \frac{\mathrm{d}v'}{\mathrm{d}r} + (1 - \mu^2) \frac{v'}{r} \right] \mathrm{d}\mu = \\
&= \frac{1}{\chi_l} \left[K_\nu(r) \left(\frac{\mathrm{d}v'}{\mathrm{d}r} - \frac{v'}{r} \right) + J_\nu(r) \frac{v'}{r} \right] = \\
&= \frac{1}{\chi_l} J_\nu(r) \left[f_\nu(r) \left(\frac{\mathrm{d}v'}{\mathrm{d}r} - \frac{v'}{r} \right) + \frac{v'}{r} \right] = J_\nu(r) \frac{1}{\tau_{\mathrm{S}}(r, \mu = \sqrt{f_\nu(r)})},
\end{aligned}$$

where all moments refer to continuum quantities (calculated in the spirit of Section 5.3.2), and $f_\nu(r) = \frac{K_\nu}{J_\nu}$ is the (conventional) Eddington factor. Including the optically thin case, one finds, to a good approximation

$$\overline{\beta_{\mathrm{c}}(r) I_{\mathrm{inc}}} \approx J_\nu(r) \frac{1 - \mathrm{e}^{-\tau_{\mathrm{S}}(r, \mu = \sqrt{f_\nu(r)})}}{\tau_{\mathrm{S}}(r, \mu = \sqrt{f_\nu(r)})},$$

and avoids the angular integration by evaluating the integrand at $\mu = \sqrt{f_\nu(r)}$[12].

Inclusion of source-function gradients. As firstly shown by Sobolev (1957) and Castor (1974), the inclusion of source-function gradients is important when calculating the line acceleration. Though a constant source function does not contribute (due to cancellation effects when integrating over $\mu \mathrm{d}\mu$, discussed previously), corresponding gradients do contribute, and might become decisive, particularly in the inner wind regime (see also Owocki and Puls, 1999). Puls and Hummer (1988) improved on the previous

[11] Escape probabilities for static atmospheres are discussed in Section 1.10.

[12] A similar reasoning yields a fair approximation for the escape probability, $\beta(r) \approx \frac{1 - \mathrm{e}^{-\tau_{\mathrm{S}}(r, \mu = \sqrt{1/3})}}{\tau_{\mathrm{S}}(r, \mu = \sqrt{1/3})}$.

works, and included corresponding continuum terms that turned out to be significant as well.

Inclusion of multiline effects. Multiline effects are essential when calculating the *total* line acceleration, $\sum_i g^i_{\rm rad}$, present in a wind (Puls, 1987). In addition to 'conventional' line-overlap effects (similar rest-wavelengths of different lines), lines can also interact with each other due to Doppler-induced frequency shifts. E.g., for the same $\nu_{\rm obs}$, there might be an interaction between a line with $\tilde{\nu}_1$ from the inner wind and a line with $\tilde{\nu}_2$ from the more outer part, if

$$\frac{\tilde{\nu}_1 - \tilde{\nu}_2}{\tilde{\nu}_1} \approx \frac{(\mu v)_2}{c} - \frac{(\mu v)_1}{c} > 0.$$

In other words, the radiation incident at $(\mu v)_2$ (determining the radiation field for the line with $\tilde{\nu}_2$) has already been processed before, by the bluewards line with $\tilde{\nu}_1$ at $(\mu v)_1$. See also Friend and Castor (1983).

Nonmonotonic velocity fields. lead to more than one resonance zone, and need to be considered, e.g., when calculating the *approximate* line acceleration in time-dependent winds. Also in this case, the basic Sobolev theory can be adapted to include such effects (see Rybicki and Hummer, 1978, for the case of two coupled resonance zones, and Puls et al., 1993, for a generalization and application to instable-wind models).

SEI (Sobolev with exact integration). When calculating line profiles (specifically, UV P Cygni lines; for the profile formation principle, see Figure 5.7), and using the SA to determine *both* the source function *and* the emergent profile, the resulting accuracy is quite low, when compared to more 'exact' methods. A better approach is to calculate the scattering integral (and thus the source function, either in a complete NLTE or a two-level approach) using the SA, and then to derive the emergent line profile from an 'exact' formal solution[13] using such a source function.

To our knowledge, this had been first noted by Hamann (1981), and was explicitly suggested by Lamers et al. (1987), under the acronym SEI. Such an approach was also, and independently, used by Puls (1987), for the case of a large number of overlapping (UV) lines, in the context of NLTE wind modeling/spectrum synthesis.

5.4.4 *Comoving Frame (CMF) Transport*

Obviously, the calculation of the radiation field in an environment with significant (supersonic) velocity fields is either time consuming, if performed in the observer's frame (many grid points, frequencies and angles), or only approximate (but fast), when done using the SA. In the latter case, there are additional difficulties when considering not only one isolated line in an optically thin continuum, but more realistic situations as occurring in NLTE atmosphere modeling (many lines, various continua, multiline effects, etc.).

A quite simple and fast way out of this dilemma is possible when the velocity field is monotonic, after transforming to the comoving frame[14].

[13] When calculating the formal solution via an integral method, it is advantageous to remap all quantities onto a microgrid of resolution $\approx v_{\rm th}/3$, to ensure a correct treatment of the resonance zone (e.g., Santolaya-Rey et al., 1997).

[14] A CMF solution is also possible for nonmonotonic velocity fields, at least in principle, but the algorithm becomes very complex.

The stationary RTE in the CMF: heuristic derivation. We start in the observer's frame, using the p-z geometry (now again for the front hemisphere only):

$$\pm\frac{\mathrm{d}I^{\pm}(z,p,\nu)}{\mathrm{d}z}=\eta_\nu\left(r,\nu\left(1-\frac{\mu v}{c}\right)\right)-\chi_\nu\left(r,\nu\left(1-\frac{\mu v}{c}\right)\right)I^{\pm}(z,p,\nu),$$

where in the following all CMF quantities are denoted by a sub- (or super-)script "0" (not to be confused with the denotation for the resonance zone), e.g., $\nu_0 \triangleq \nu_{\mathrm{CMF}} = \nu\,(1-\mu v/c)$.

A velocity field produces Doppler shifts, aberration and advection terms (discussed later in this section); formally, all of these are $O(v/c)$ effects, but for lines the Doppler shifts become already significant if $v = O(v_{\mathrm{th}})$, due to the rapid change of the profile function. In the following heuristic approach, we concentrate on these Doppler shifts alone and neglect the rest (see also Lucy, 1971).

Since $\nu_0 = \nu_0(\nu, z) = \nu\,(1-\mu v/c)$, the spatial derivative in the RTE needs to account for the change of ν_0 with z (see Figure 5.8):

$$\left.\frac{\mathrm{d}}{\mathrm{d}z}\right|_{\nu}=\left.\frac{\partial}{\partial z}\right|_{\nu_0}+\left.\frac{\partial}{\partial \nu_0}\right|_{z_0}\left.\frac{\partial \nu_0}{\partial z}\right|_{\nu},\ \text{with}\ \left.\frac{\partial \nu_0}{\partial z}\right|_{\nu}=-\frac{\nu}{c}\frac{\partial(\mu v)}{\partial z}\overset{O(v/c)}{\approx}\mp\frac{\nu_0}{c}\tilde{Q}(r,\mu). \tag{5.22}$$

Here, we have approximated $r \approx r_0$ and $\mu \approx \mu_0$, and accounted for the fact that when using $z > 0$ exclusively, $\partial(\mu v)/\partial z = \pm\,\tilde{Q}(r,\mu)$ for $\mu > 0$ and $\mu < 0$, respectively. $\tilde{Q}$ corresponds to our 'conventional' Q (e.g., (5.18)), but is evaluated using v instead of v'.

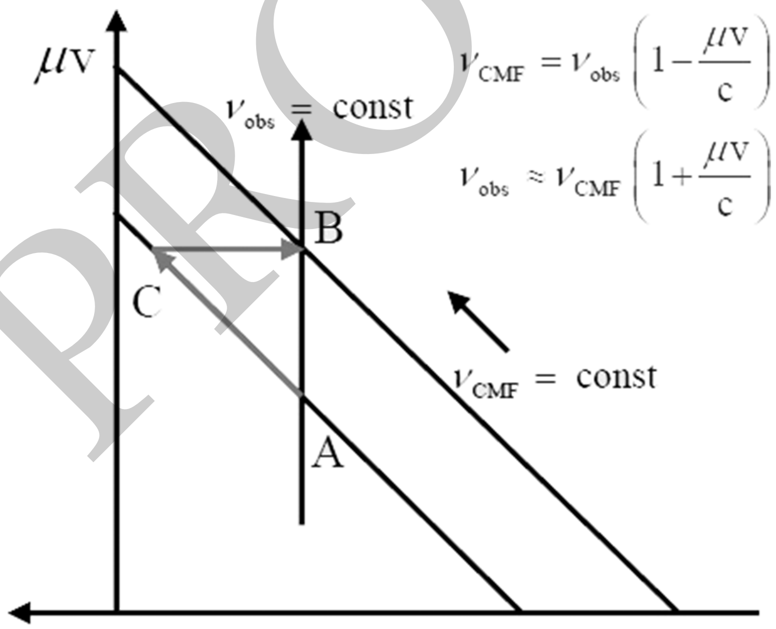

FIGURE 5.8. Transformation of the observer's frame spatial derivative (5.22), $(\mathrm{d}/\mathrm{dz})_{\nu=\mathrm{const}}$: While in the observer's frame we proceed from A to B with $\nu = \mathrm{const}$, and in the CMF we proceed via A $\overset{\nu_0=\mathrm{const}}{\rightarrow}$ C, followed by C $\overset{z_0\approx z=\mathrm{const}}{\rightarrow}$ B.

Thus, the RTE becomes

... in spherical symmetry, and using a p-z geometry, with $r_0 \approx r$, $z_0 \approx z$, $\mu_0 \approx \mu$,

$$\pm\frac{\partial I_0^{\pm}(z,p,\nu_0)}{\partial z} - \frac{\nu_0\tilde{Q}(r,\mu)}{c}\frac{\partial I_0^{\pm}(z,p,\nu_0)}{\partial \nu_0} = \eta_0(r,\nu_0) - \chi_0(r,\nu_0)I_0^{\pm}(z,p,\nu_0). \tag{5.23}$$

While the spatial derivative enters with $\pm$ for outwards and inwards radiation, respectively, the frequency derivative has the same sign in both cases. This, again, is due to the fact that the gradient of (μv) is always positive in a spherically expanding medium (as long as $v(r)$ is monotonically increasing), irrespective of direction.

... in spherical symmetry with $r_0 \approx r$, $\mu_0 \approx \mu$

$$\begin{aligned}\mu\frac{\partial I_0(r,\mu,\nu_0)}{\partial r} &+ \frac{(1-\mu^2)}{r}\frac{\partial I_0(r,\mu,\nu_0)}{\partial \mu} - \frac{\nu_0\tilde{Q}(r,\mu)}{c}\frac{\partial I_0(r,\mu,\nu_0)}{\partial \nu_0}\\ &= \eta_0(r,\nu_0) - \chi_0(r,\nu_0)I_0(r,\mu,\nu_0),\end{aligned}$$

... and in plane-parallel symmetry with $z_0 \approx z$, $\mu_0 \approx \mu$

$$\mu\frac{\partial I_0(z,\mu,\nu_0)}{\partial z} - \frac{\nu_0\mu^2(\mathrm{d}v/\mathrm{d}z)}{c}\frac{\partial I_0(z,\mu,\nu_0)}{\partial \nu_0} = \eta_0(z,\nu_0) - \chi_0(z,\nu_0)I_0(z,\mu,\nu_0).$$

- The full transformation of the RTE (including time-dependent terms) can be found, e.g., in Castor (1972).
- Mihalas et al. (1976) showed that aberration terms (involving changes in direction μ) and advection terms (arising 'from gradients or from a "sweeping up" of radiation by the transformation' to the CMF) can be neglected when $v \ll c$ as considered here, while the frequency derivatives are most important. Thus far, the preceding equations are sufficient as long as $v \ll c$ (but: SN remnants with $v/c \lesssim 0.04 \ldots 0.15$(!)).
- In the preceding equations, particularly I_0, η_0, and χ_0 are comoving frame variables, and η_0 and χ_0 are *isotropic*.
- Consequently, for each line (if treated as a single one), only a small frequency range covering the variation of $\phi(\approx \pm 3v_{\mathrm{th}})$ needs to be considered.
- If only one line is considered, the RT is performed exclusively in the corresponding resonance zone.
- The CMF RTE is a partial differential equation (PDE) of hyperbolic type, and poses an initial boundary value problem, i.e., it requires boundary conditions in space and initial values in frequency.
- For larger frequency ranges, it might be useful to differentiate via

$$\frac{\nu_0\tilde{Q}(r,\mu)}{c}\frac{\partial}{\partial \nu_0} = \frac{\tilde{Q}(r,\mu)}{c}\frac{\partial}{\partial \ln \nu_0}.$$

Characteristics of the homogeneous equation. Often, the CMF equation of RT (e.g., (5.23)) is expressed in terms of Doppler units with respect to v_∞, $x_0 = \nu_0 - \tilde{\nu}/\Delta\nu_\infty$, and $\Delta\nu_\infty = \nu_0\ v_\infty/c$, where $\tilde{\nu}$ is an arbitrary reference frequency close to ν_0 (e.g., the line-center frequency, if only one line is considered). Measuring v in units of v_∞ ($v'' = v/v_\infty$), and accounting for

$$\mathrm{d}x_0 = \frac{c}{v_\infty}\frac{\tilde{\nu}}{\nu_0}\frac{\mathrm{d}\nu_0}{\nu_0} \approx \frac{c}{v_\infty\nu_0}\mathrm{d}\nu_0 = \frac{\mathrm{d}\nu_0}{\Delta\nu_\infty},$$

we find

$$\pm\frac{\partial I_0^{\pm}(z,p,x_0)}{\partial z} - P(r,\mu)\frac{\partial I_0^{\pm}(z,p,x_0)}{\partial x_0} = \eta_0(r,x_0) - \chi_0(r,x_0)I_0^{\pm}(z,p,x_0) \tag{5.24}$$

with

$$P(r,\mu) = \frac{\mathrm{d}(\mu v'')}{\mathrm{d}z} = \left(\mu^2\frac{\mathrm{d}v''}{\mathrm{d}r} + (1-\mu^2)\frac{v''}{r}\right).$$

The characteristics of the homogeneous (RHS = 0) PDE are the curves (generally: hypersurfaces) along which $I_0^{\pm}$ remains constant if there is no absorption/emission, and need to be known, e.g., if we want to investigate the interaction (irradiation) of two lines (from red edge of first to blue edge of second line), in case of a negligible continuum. For the type of PDE considered here, these characteristics are given by (see standard textbooks)

$$\frac{\mathrm{d}x_0}{\mathrm{d}z} = \mp P(z),$$

and integration results in

$$0 < \Delta x_0 = x_{0,B} - x_0 = \mp\int_z^{z_B} P(z)\mathrm{d}z = \mp\left[\mu v''(z_B) - \mu v''(z)\right] = \mp\Delta\mu v''. \text{ Thus,}$$
$$I_0^{\pm}(\mu v''(z), x_0) = I_0^{\pm}(\mu v''(z_B), x_{0,B}) = I_0^{\pm}(\mu v''(z) \mp \Delta x_0, x_0 + \Delta x_0).$$

See Figure 5.9. Without absorption and emission, *all* photons are 'only' redshifted with regard to the CMF, from $x_0 + \Delta x_0$ to x_0, both when propagating outwards from $\mu v''(z) - \Delta x_0$ to $\mu v''(z)$, and when propagating inwards from $\mu v''(z) + \Delta x_0$ to $\mu v''(z)$. The corresponding *observer's frame* intensity at x, $I^{\pm}(z,x)$, remains constant, of course.

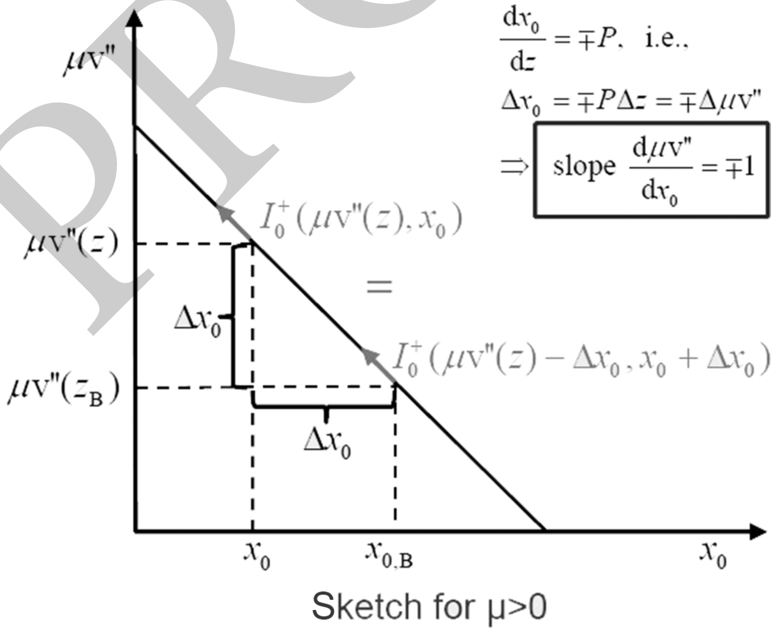

FIGURE 5.9. Characteristics of the homogeneous RTE in the CMF (5.24). See text.

Sobolev limit. From the comoving frame RTE, (5.24), one can also derive the Sobolev limit. Since we are in the CMF, this equation needs to be solved only in those regions of x_0 where the profile function is nonnegligible. This, however, corresponds to the resonance zone, where the SA assumes that all macrovariables (except v) are spatially constant. In this spirit, when neglecting the spatial derivative, the Sobolev limit can be easily obtained.

We will show this here for the case of one purely absorbing line with transition frequency $\tilde{\nu}$ and positive μ (no continuum), the generalization is left as an exercise for the reader (or see Lucy, 1971; Puls, 1991). From

$$-P(r,\mu)\frac{\partial I_0^+(z,p,x_0)}{\partial x_0} = -\chi_0(r,x_0)I_0^+(z,p,x_0),$$

where (z,r,μ) refer to the resonance zone, we obtain[15]

$$\ln\left[I_0^+(z,p,x_0)/I_0^{\rm inc}(z,p,x_{0,B})\right] = \frac{\bar{\chi}_{\rm L}(r)}{\Delta\nu_\infty P(r,\mu)}\int\limits_{x_{0,B}}^{x_0}\phi(x){\rm d}x$$
$$I_0^+(z,p,x_0) = I_0^{\rm inc}(z,p,x_{0,B})\,\exp\left[-\tau_S(r,\mu)\,\Phi(x_0)\right],$$

q.e.d. (One might compare with (5.19), and note that the preceding solution is already evaluated in the resonance zone.)

Solution methods. The basic approach to numerically solve the CMF RTE in spherically expanding atmospheres is similar to the treatment of the (quasi-)isotropic continuum (Section 5.3.2).

Method 1 (formal solution): Here, 'only' the discretized CMF RTE for the Feautrier variables u^0 and v^0 is solved, with $u^0 = \frac{1}{2}(I_0^+ + I_0^-)$ and $v^0 = \frac{1}{2}(I_0^+ - I_0^-)$. In p-z geometry, we thus have (cf. (5.24))

$$\begin{aligned}\frac{\partial u^0}{\partial z} - P\frac{\partial v^0}{\partial {\rm x}_0} &= -\chi_0 v^0\\ \frac{\partial v^0}{\partial z} - P\frac{\partial u^0}{\partial {\rm x}_0} &= \chi_0(S_0 - u^0),\end{aligned} \tag{5.25}$$

where x_0 is the CMF frequency in Doppler units with respect to v_∞, and $P(r,\mu) = ({\rm d}\mu v/v_\infty)/{\rm d}z = \left(\mu^2\frac{{\rm d}\mu v/v_\infty}{{\rm d}r} + (1-\mu^2)\frac{v/v_\infty}{r}\right)$.

(5.25) is a system of two coupled, first-order PDEs, where (almost) all variables are to be evaluated in the CMF and depend on z (as a function of impact parameter p), r and x_0.

Spatial boundary values are specified as before (see Section 5.3.2), plus a 'blue-wing' boundary condition at the bluemost frequency, from the solution of a pure continuum transport. Special attention needs to be paid if the integration extends over a larger frequency range (more than one line), by a careful formulation of the outer boundary condition for optically thick conditions[16] (e.g., bluewards from the He II Lyman edge); otherwise, numerical artefacts might be created and transported through the spatial and frequency grid.

[15] Since x_0 is in units of v_∞, the corresponding profile function is normalized with regard to $\Delta\nu_\infty$

[16] Unfortunately, such formulations are usually not published.

The preceding PDEs are discretized using either of the following:

- A fully implicit scheme[17] (second-order in space, first-order in frequency), that is unconditionally stable (Mihalas et al., 1975).
- A semi-implicit (Crank–Nicholson) scheme, which is of higher accuracy, since it is of second order in frequency. If used in the formulation by Hamann (1981) (and *not* in the formulation by Mihalas et al., 1975), this is unconditionally stable as well.

Method 2 (variable Eddington factors): Here one uses the CMF-moments equations to obtain the moments of the radiation field (in the CMF). Contrasted with the corresponding observer's frame equations for isotropic opacities/emissivities (Section 5.3.1), also the third moment of the specific intensity, N^0_ν, enters the equations:

$$\frac{1}{r^2}\frac{\partial\left(r^2 H^0_\nu\right)}{\partial r} - \frac{\nu_0}{c}\left[\frac{v}{r}\frac{\partial(J^0_\nu - K^0_\nu)}{\partial\nu_0} + \frac{\mathrm{d}v}{\mathrm{d}r}\frac{\partial K^0_\nu}{\partial\nu_0}\right] = \eta_0(\nu_0) - \chi_0(\nu_0)J^0_\nu$$

$$\frac{\partial K^0_\nu}{\partial r} + \frac{3K^0_\nu - J^0_\nu}{r} - \frac{\nu_0}{c}\left[\frac{v}{r}\frac{\partial(H^0_\nu - N^0_\nu)}{\partial\nu_0} + \frac{\mathrm{d}v}{\mathrm{d}r}\frac{\partial N^0_\nu}{\partial\nu_0}\right] = -\chi_0(\nu_0)H^0_\nu$$

By means of the sphericality factor q_ν (5.13) and the Eddington factors $f^0_\nu = K^0_\nu/J^0_\nu$ and $g^0_\nu = N^0_\nu/H^0_\nu$ (calculated from the formal solution), we obtain again a coupled system of first-order PDEs for $r^2J^0_\nu$ and $r^2H^0_\nu$, that can be solved by discretization:

$$-\frac{\partial\left(r^2H^0_\nu\right)}{\partial r} + \frac{\nu_0}{c}\left[\frac{\mathrm{d}v}{\mathrm{d}r} - \frac{v}{r}\right]\frac{\partial\left(f^0_\nu r^2 J^0_\nu\right)}{\partial\nu_0} + \frac{\nu_0}{c}\frac{v}{r}\frac{\partial\left(r^2J^0_\nu\right)}{\partial\nu_0} = \chi_0(\nu_0)\left(r^2J^0_\nu - r^2S^0_\nu\right)$$

$$-\frac{\partial\left(q_\nu f^0_\nu r^2 J^0_\nu\right)}{q_\nu\partial r} + \frac{\nu_0}{c}\left[\frac{\mathrm{d}v}{\mathrm{d}r} - \frac{v}{r}\right]\frac{\partial\left(g^0_\nu r^2 H^0_\nu\right)}{\partial\nu_0} + \frac{\nu_0}{c}\frac{v}{r}\frac{\partial\left(r^2H^0_\nu\right)}{\partial\nu_0} = \chi_0(\nu_0)r^2H^0_\nu$$

In this case, a Rybicki scheme might be used if the source function can be separated into scattering and true absorption/emission components[18].

Radiative acceleration. To calculate the radiative acceleration, in the observer's frame we would need to evaluate (see (5.11))

$$\mathbf{g}_{\mathrm{rad}} = \frac{1}{c\rho}\int \mathrm{d}\nu \oint \left(\chi\left(\nu(1-\mu v/c)\right)I_\nu(\mu) - \eta\left(\nu(1-\mu v/c)\right)\right)\mathbf{n}\mathrm{d}\Omega,$$

since the (line-)opacities and emissivities are angle dependent when a velocity field is present.

Because of the isotropy of χ^0_ν and η^0_ν in the comoving frame, however, this expression becomes considerably simplified when evaluated in the CMF,

$$\mathbf{g}^0_{\mathrm{rad}} = \frac{4\pi}{c\rho}\int \chi^0_\nu H^0_\nu \mathrm{d}\nu, \quad \text{since} \oint \chi^0_\nu I_0(\mu,\nu_0)\mathbf{n}\mathrm{d}\Omega = 4\pi\chi^0_\nu H^0_\nu, \quad \text{and} \oint \eta^0_\nu \mathbf{n}\mathrm{d}\Omega = 0.$$

Interestingly (and fortunately), one can show (e.g., Mihalas, 1978, chapter 15.3), that this expression is not only valid when used within the fluid frame (=CMF) equations of motion, but also, to order (v/c), in the corresponding inertial frame formulation. Namely, when the moments of the radiation field contained in the coupled matter–radiation equation of motion are expressed in terms of their CMF counterparts, and if the CMF moments equations (which we have just shown) are used, a delicate cancellation of

[17] For this scheme, an almost optimum local approximate lambda operator (ALO) can be calculated in parallel (see the next section and Puls, 1991).

[18] See equations (1.46) and (1.47) in Section 1.9.4.

terms ensures that also in the inertial frame the preceding expression for $\mathbf{g}^0_{\rm rad} \overset{O(v/c)}{\rightarrow} \mathbf{g}_{\rm rad}$ can be used for the radiative acceleration.

5.5 Accelerated Lambda Iteration (ALI) and 'Preconditioning'

The content of this section is not *directly* related to radiative transfer, but important if an NLTE treatment[19] of the plasma is required. This is particularly true for the atmospheres of hot stars, where the radiative rates dominate over the collisional ones in the line-forming region, due to a strong radiation field (and low densities in the stellar wind). Part of this section overlaps with the contents of Sections 3.7 and 3.8, but most issues are discussed here with special emphasis on the conditions in rapidly expanding atmospheres, providing an additional perspective.

Basically, there are two methods to obtain a consistent solution for the radiation field and the occupation numbers: (i) the complete-linearization method (Auer and Mihalas, 1969), used, e.g., in CMFGEN (Appendix A); and (ii) the ALI (Werner and Husfeld, 1985), used, e.g., in PoWR, WM-basic and FASTWIND (also Appendix A). Generally, the ALI method is easier to programme and has a faster performance per iteration step, but often requires more iterations than complete linearization.

The basic idea of the original (not accelerated) lambda iteration is as follows: One (a) starts with guessing values for the occupation numbers (e.g., from LTE or simplified NLTE conditions); (b) calculates corresponding opacities and source functions; (c) solves the RTE and calculates the mean intensities and scattering integrals; and (d) solves the rate equations involving J_ν and $\bar{J}$, i.e., calculates new occupation numbers. Subsequently, steps (b) to (d) are carried out again, and the process is iterated until (at least in terms of wishful thinking) convergence is obtained.

In practice, however, the convergence of this iteration (if at all achieved) is particularly slow for optically thick, scattering dominated processes, and it is rather difficult or even impossible to define an appropriate convergence criterion. These difficulties base on the fact that during each iteration, information is propagated only over $\Delta\tau_\nu \approx 1$. The *Accelerated* Lambda Iteration has been developed to get rid of these problems.

5.5.1 *A Simple Example*

To obtain more insight into the difficulties outlined earlier, we first concentrate on a simple showcase, namely a purely scattering line (e.g., a UV-resonance line) in Sobolev approximation. Then, we have the following:

(i) $S = \bar{J}$	Most simple 'rate equation' (e.g., from two-level atom without collisions)
(ii) $\bar{J} = (1-\beta)S + \beta_{\rm c} I_{\rm core}$	'Formal solution' (Sobolev solution for line transfer in optically thin continua, see (5.20))

Let's assume that the opacities are known and remain constant over the iteration, which is not too wrong for resonance lines.

Method A: Using (i) and (ii) in parallel, it is possible to obtain a consistent analytic solution,

$$S = (1-\beta)S + \beta_{\rm c} I_{\rm core} \Rightarrow S = \frac{\beta_{\rm c} I_{\rm core}}{\beta} \text{ (balance between irradiation and escape)}$$

[19] This accounts for the coupling between radiation field and occupation numbers via rate equations.

Method B: Alternatively, we apply the lambda iteration. We start with a guess value for the source function, S^0, and calculate the scattering integral, $\bar{J}^0$, using (ii). Then we determine a new iterate for the source function, S^1, using (i):

$$S^1 = (1-\beta)S^0 + \beta_{\rm c} I_{\rm core}.$$

Generally,

$$\left.\begin{aligned} S^n &= (1-\beta)S^{n-1} + \beta_{\rm c} I_{\rm core} \\ S^{n-1} &= (1-\beta)S^{n-2} + \beta_{\rm c} I_{\rm core} \end{aligned}\right\} S^n - S^{n-1} := \Delta S^n = (1-\beta)\Delta S^{n-1}, \qquad (5.26)$$

and for optically thick lines where $\beta \rightarrow 1/\tau_S$ and thus $\beta \ll 1$, it turns out that $\Delta S^n \approx \Delta S^{n-1}$, i.e., no reasonable convergence criterion can be defined.

From this example, two questions are obvious: When do we consider the solution as converged? And how does the direct solution (*Method A*) and the Lambda-iterated solution (*Method B*) compare? To answer these questions, we investigate the limiting value of S^n for $n \rightarrow \infty$.

$$\begin{aligned} S^n &= (1-\beta)S^{n-1} + \beta_{\rm c} I_{\rm core} = (1-\beta)\left[(1-\beta)S^{n-2} + \beta_{\rm c} I_{\rm core}\right] + \beta_{\rm c} I_{\rm core} = \\ &= \ldots = (1-\beta)^n S^o + \beta_c I_{core}\left[(1-\beta)^{n-1} + (1-\beta)^{n-2} + \cdots + 1\right]. \end{aligned}$$

Accounting for $\sum\limits_{\rm i=0}^{\rm n-1} q^i = \frac{1-q^n}{1-q}$, we obtain

$$S^n = (1-\beta)^n S^0 + \beta_{\rm c} I_{\rm core} \frac{1-(1-\beta)^n}{\beta} \stackrel{n\rightarrow\infty}{\rightarrow} \frac{\beta_{\rm c} I_{\rm core}}{\beta},$$

i.e., indeed the Lambda-iterated solution (from *Method B*) converges (very slowly) to the correct one from *Method A* (and becomes independent from the start value).

How many iteration steps are required? For $\beta \ll 1$, we can approximate $(1-\beta)^n \approx (1-n\beta)$, and to ensure convergence, we must have $(1-\beta)^n \rightarrow 0$, i.e., $n \gtrsim 1/\beta \rightarrow \tau_S$. Thus, we would need roughly the same number of iterations as the size of τ_S, which (i) can be very large for resonance lines, $n \approx \tau_S$ up to $O(10^5 \ldots 10^6)$, and (ii) shows that indeed, per iteration step, information corresponding to only $\Delta\tau = 1$ is propagated.

5.5.2 *Accelerated Lambda Iteration*

Generalizing the aforementioned simplified problem, we need to fulfil the following requirement for a consistent solution of the coupled problem (RT and rate equations)

$$S^n \overset{\text{via rate equations}}{\overbrace{=}} f(J^n) = f\left(\overset{\text{formal solution}}{\overbrace{\Lambda\left[S^n\right]}}\right),$$

which is a nonlinear and, except for the Sobolev case, nonlocal problem. In contrast, the lambda iteration provides us with

$$S^n = f(J^{n-1}) = f(\Lambda\left[S^{n-1}\right]),$$

which displays the well-known convergence problems. We stress that Λ is an affine operator[20], due to the boundary conditions.

[20] Linear transformation plus displacement.

In the following, we consider continuum (J) and line problems ($\bar{J}$) in parallel. A generalization of results for continuum quantities to line conditions is straightforward, by solving for all line frequencies and integrating over the profile function.

For values on a 1-D spatial grid (with N grid points), we may rewrite the formal solution of RT in form of an affine relation,

$$\mathbf{J} = \mathbf{\Lambda} \cdot \mathbf{S} + \mathbf{\Phi},$$

where $\mathbf{J}$, $\mathbf{S}$ and $\mathbf{\Phi}$ are vectors of length N, and $\mathbf{\Lambda}$ is a matrix with $N \times N$ elements. $\mathbf{\Phi}$ corresponds to the boundary conditions, $\mathbf{J}(\mathbf{S} = \mathbf{0})$.

If required, the elements Φ_i and Λ_{ij} might be derived (in 1-D) from $N + 1$ formal solutions for $\mathbf{S} = \mathbf{0}$, $\mathbf{S} = \mathbf{e}_1, \ldots, \mathbf{S} = \mathbf{e}_N$, respectively, where

$$\mathbf{e}_j = (0, \ldots, 0, 1, 0, \ldots, 0)^T$$

is the unit vector in direction j.

ALI is based on the idea of operator splitting (e.g., Cannon, 1973), namely to split[21]

$$\mathbf{\Lambda} = \mathbf{\Lambda}^A + \left(\mathbf{\Lambda} - \mathbf{\Lambda}^{\mathbf{A}}\right),$$

the lambda operator into an approximate operator (with a linear component that should be easily invertible) and a rest part. Then we can approximate

$$\mathbf{J}^n \approx \mathbf{\Lambda}^A \left[\mathbf{S}^n\right] + \left(\mathbf{\Lambda} - \mathbf{\Lambda}^A\right) \left[\mathbf{S}^{n-1}\right],$$

where equality is obtained for $n \to \infty$, when $\mathbf{S}^{n-1} \to \mathbf{S}^n$.

This is the essential clue, since now we have a relation (at step n) between $\mathbf{J}^n$ and $\mathbf{S}^n$, and not only between $\mathbf{J}^{n-1}$ and $\mathbf{S}^{n-1}$.

Also the ALO, $\mathbf{\Lambda}^A$, needs to be of affine type, i.e., $\mathbf{\Lambda}^A[\mathbf{S}] = \mathbf{\Lambda}^* \cdot \mathbf{S} + \mathbf{\Phi}^*$, but even then

$$\begin{aligned} \mathbf{J}^n &= \left[\mathbf{\Lambda}^* \cdot \mathbf{S}^n + \mathbf{\Phi}^*\right] + \mathbf{J}^{n-1} - \left[\mathbf{\Lambda}^* \cdot \mathbf{S}^{n-1} + \mathbf{\Phi}^*\right], \text{ i.e.,} \\ \mathbf{J}^n &= \mathbf{\Lambda}^* \cdot \mathbf{S}^n + \mathbf{\Delta J}^{n-1}, \text{ with } \mathbf{\Delta J}^{n-1} = \mathbf{J}^{n-1} - \mathbf{\Lambda}^* \cdot \mathbf{S}^{n-1}, \end{aligned} \tag{5.27}$$

only the linear part of the ALO, $\mathbf{\Lambda}^*$, needs to be specified, assuming that $\mathbf{\Phi}^*$ remains constant over the iteration.

We note that $\mathbf{\Delta J}^{n-1}$ depends only on $\mathbf{S}^{n-1}$, and can be calculated from the formal solution for $\mathbf{J}^{n-1}$ (and specified $\mathbf{\Lambda}^*$).

ALI in practice. To illustrate how ALI works in practice, we consider a continuum problem with scattering, or – again – a two-level atom,

$$\mathbf{S} = \boldsymbol{\xi}\mathbf{J} + \boldsymbol{\psi},$$

where $\boldsymbol{\xi}$ is a diagonal matrix (containing the scattering fractions, $0 \le \xi_{ii} \le 1$), and $\boldsymbol{\psi}$ is a vector (containing the Planck functions). Then,

$$\mathbf{S}^n = \boldsymbol{\xi}\left(\mathbf{\Lambda}^*\mathbf{S}^n + \mathbf{\Delta}\boldsymbol{J}^{n-1}\right) + \boldsymbol{\psi},$$

[21] Similar to the Jacobi iteration in boundary value problems.

and we obtain an explicit expression for $\mathbf{S}^n$,

$$\mathbf{S}^n = (\mathbf{1} - \boldsymbol{\xi}\boldsymbol{\Lambda}^*)^{-1} \left(\boldsymbol{\xi}\boldsymbol{\Delta}\mathbf{J}^{n-1} + \boldsymbol{\psi}\right) = (\mathbf{1} - \boldsymbol{\xi}\boldsymbol{\Lambda}^*)^{-1} \left(\boldsymbol{\xi}(\boldsymbol{\Lambda} - \boldsymbol{\Lambda}^*)\mathbf{S}^{n-1} + \boldsymbol{\psi}\right), \qquad (5.28)$$

which constitutes the ALI scheme for simple source functions (those that can be analytically separated into a scattering and thermal part).

With $\boldsymbol{\Delta}\mathbf{S}^n := \mathbf{S}^n - \mathbf{S}^\infty$ (deviation from the 'true' source function $\mathbf{S}^\infty$, in contrast to the definition in (5.26)), we finally find (after a few algebraic manipulations)

$$\boldsymbol{\Delta}\mathbf{S}^n = \mathbf{A}\boldsymbol{\Delta}\mathbf{S}^{n-1}, \qquad \text{with amplification matrix} \quad \mathbf{A} = (\mathbf{1} - \boldsymbol{\xi}\boldsymbol{\Lambda}^*)^{-1} (\boldsymbol{\xi}(\boldsymbol{\Lambda} - \boldsymbol{\Lambda}^*)).$$

One can show that under typical conditions $\mathbf{A}$ has a complete set of real and orthogonal eigenvectors, and real eigenvalues λ (e.g., Puls and Herrero, 1988). Expanding $\boldsymbol{\Delta}\mathbf{S}$ in terms of these eigenvectors, for large n we obtain $\boldsymbol{\Delta}\mathbf{S}^n \approx \lambda_{\max}^n \boldsymbol{\Delta}\mathbf{S}^0$, where $\lambda_{\max} = \pm\max(|\lambda_i|)$, and the minus sign applies when the corresponding eigenvalue is negative. Thus, the ALI scheme converges if $|\lambda_{\max}| < 1$. For *static* problems, Olson et al. (1986) showed that in particular

$$|\lambda_{\max}| < 1, \qquad \text{if} \quad \boldsymbol{\Lambda}^* = \text{diag(linear part of}\,\boldsymbol{\Lambda}).$$

A very elegant method to calculate the corresponding $\boldsymbol{\Lambda}^*$ has been provided by Rybicki and Hummer (1991, appendix). For the case of CMF line transfer, on the other hand, Puls (1991) developed an almost optimum, purely local ALO (see Figure 5.10).

- Both of these ALOs can be calculated in parallel with the corresponding RT, on very fast timescales.
- Since the CMF line transfer has an essentially local character in rapidly expanding atmospheres (taking place only in the narrow resonance zone), a local ALO is sufficient when solving the rate equations under such conditions.
- For local ALOs, an overestimation of the exact diagonal leads to divergence in most cases.

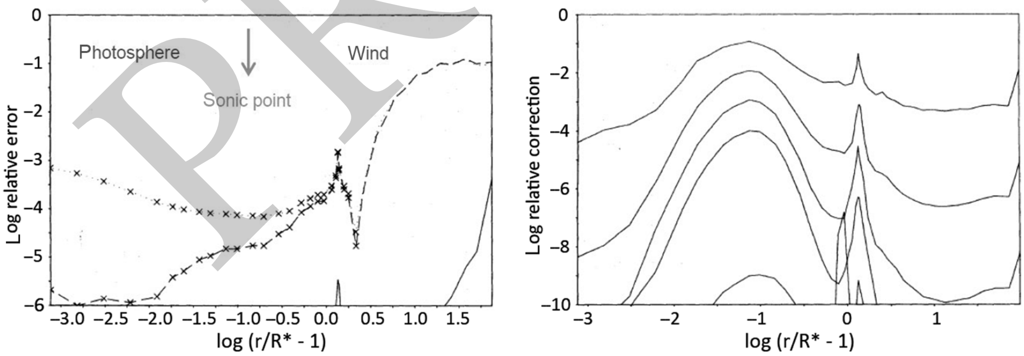

FIGURE 5.10. Local ALO, $\boldsymbol{\Lambda}^*$, from Puls (1991), and corresponding ALI cycle, for a CMF line source function in an expanding atmosphere. The displayed example refers to a strong, purely scattering line. *Left*: relative deviation (absolute value, logarithmic) among (i) solid – the exact diagonal of the Lambda operator and $\boldsymbol{\Lambda}^*$ (relative differences mostly below 10^{-6}); (ii) dotted – the exact diagonal and $(1 - \beta)$ (cf. 5.29); and (iii) dashed – the exact diagonal and $(1 - \beta - \bar{U})$, when using the SA with continuum. Since $(1 - \beta)$ overestimates the exact diagonal in most regions (not visible since absolute values are displayed), it cannot be used as an ALO. *Right*: Relative corrections $\Delta S^n/S^n$ for subsequent iterations, as a function of radius. Adapted from Puls (1991). Reproduced with permission © ESO.

For non-local ALOs and more sophisticated iteration schemes (e.g., required in multi-D calculations), we refer to Trujillo Bueno and Fabiani Bendicho (1995) and references therein. See also Hennicker et al. (2018).

Comparison between ALI scheme and Sobolev approach (line case). Assuming a local ALO, for each depth point we have the correspondence

$$\left.\begin{array}{ll}\text{ALI:} & \bar{J}^n = \Lambda^* S^n + \underbrace{\Delta \bar{J}^{n-1}}_{\bar{J}^{n-1} - \Lambda^* S^{n-1}} \\ \text{Sobolev:} & \bar{J}^n = (1-\beta) S^n + \beta_{\mathrm{c}} I_{\mathrm{core}}\end{array}\right\} \Lambda^* \stackrel{\Delta}{=} (1-\beta), \text{ and } \Delta \bar{J}^{n-1} \stackrel{\Delta}{=} \beta_{\mathrm{c}} I_{\mathrm{core}} \tag{5.29}$$

We note that when comparing with the SA with continuum, this correspondence would read $\Lambda^* \stackrel{\Delta}{=} (1-\beta-\bar{U})$. See Figure 5.10 and (5.21).

5.5.3 *Implementation into Rate Equations – 'Preconditioning'*

In the last section of this overview, we discuss how the ALI approach is implemented into the rate equations. We start with the definition of the so-called net line rate, Z_{ul}, quantifying the net transition rate for a line transition with upper and lower levels u, l, and corresponding occupation numbers, n_u, n_l, respectively:

$$Z_{ul} = n_u A_{ul} \left(1 - \frac{\bar{J}}{S}\right),$$

where A_{ul} is the Einstein coefficient for spontaneous emission, and $Z_{ul} > 0$ if the downward transitions dominate. The corresponding line source function is given by

$$S = \frac{n_u A_{ul}}{n_l B_{lu} - n_u B_{ul}},$$

with Einstein coefficients for absorption, B_{lu}, and induced emission, B_{ul}.

Without ALI, and applying the conventional (not accelerated) lambda iteration, S^n would be calculated using $\bar{J}^{n-1}$ in the rate equations,

$$\begin{aligned}\frac{\bar{J}^{n-1}}{S^n} &= \bar{J}^{n-1}\left(\frac{n_l B_{lu} - n_u B_{ul}}{n_u A_{ul}}\right)\\ \Rightarrow Z_{ul} &= n_u \cdot \underbrace{\left(A_{ul} + B_{ul}\bar{J}^{n-1}\right)}_{\text{downward line rate}} - n_l \cdot \underbrace{\left(B_{lu}\bar{J}^{n-1}\right)}_{\text{upward line rate}},\end{aligned}$$

where the second equation denotes the downward and upward rates for the considered line transition within the rate matrix.

With ALI and local ALO, S^n is calculated using $\bar{J}^n = \Lambda^* S^n + \Delta\bar{J}^{n-1}$:

$$\begin{aligned}\frac{\bar{J}^n}{S^n} &= \Lambda^* + \frac{\Delta\bar{J}^{n-1}}{S^n}\\ \Rightarrow Z_{ul} &= n_u A_{ul}\left(1 - \Lambda^* - \frac{\Delta\bar{J}^{n-1}}{S^n}\right) =\\ &= n_u \cdot \underbrace{\left(A_{ul}(1-\Lambda^*) + B_{ul}\Delta\bar{J}^{n-1}\right)}_{\text{downward line rate}} - n_l \cdot \underbrace{\left(B_{lu}\Delta\bar{J}^{n-1}\right)}_{\text{upward line rate}}\end{aligned}$$

A comparison of the line rates,

$$A_{ul} \to A_{ul}(1 - \Lambda^*)$$
$$B_{ul}\bar{J}^{n-1} \to B_{ul}\Delta\bar{J}^{n-1}$$
$$B_{lu}\bar{J}^{n-1} \to B_{lu}\Delta\bar{J}^{n-1},$$

shows that all rates become smaller in the ALI formulation, since the inefficient part (the optically thick line core, where upward and downward rates are equal) is analytically cancelled, and only the efficient part (the optically thin wings) survives. This modification of the line rates when using the ALI scheme has been named 'preconditioning' by Rybicki and Hummer (1991), and the corresponding rates are sometimes called 'effective' or 'reduced' rates.

Reduced rates for Sobolev transport. Similar to the preceding reasoning, we now investigate the consequence of using the SA scattering integrals in the rate equations,

$$\begin{aligned} Z_{ul} &= n_u\left(A_{ul} + B_{ul}\bar{J}\right) - n_l B_{lu}\bar{J} = \\ &= n_u\left(A_{ul} + B_{ul}\left[(1-\beta)S + \beta_\mathrm{c} I_\mathrm{core}\right]\right) - n_l B_{lu}\left[(1-\beta)S + \beta_\mathrm{c} I_\mathrm{core}\right] = \cdots = \\ &= n_u\left(A_{ul}\beta + B_{ul}\beta_\mathrm{c} I_\mathrm{core}\right) - n_l B_{lu}\beta_\mathrm{c} I_\mathrm{core}. \end{aligned}$$

Also here, the contribution from the optically thick core cancels analytically. By comparing this contribution with the analogous result from the ALI approach, we again find the correspondence (see (5.29))

$$\Lambda^* \triangleq (1-\beta), \qquad \text{and} \quad \Delta\bar{J}^{n-1} \triangleq \beta_\mathrm{c} I_\mathrm{core}.$$

If one would use the Sobolev approximation with continuum (5.21), this correpondence would read

$$\Lambda^* \triangleq (1-\beta-\bar{U}), \qquad \text{and} \quad \Delta\bar{J}^{n-1} \triangleq \beta_\mathrm{c}(r) I_\mathrm{inc} + \bar{U} S_c.$$

5.6 Further Issues and Applications

Due to space (and time) limitations, a variety of additional issues could not be treated in this overview. In the following, we will provide important keywords in this context (certainly not a complete list), marked in italics if *directly* related to specific RT problems in early-type stellar atmospheres.

- Temperature structure: radiative equilibrium vs. thermal electron balance
- Energy equation, adiabatic expansion and cooling in the outermost wind
- *LDI and impact of a diffuse radiation field*
- Inhomogeneous winds, shocks and X-ray emission
- Examples/applications
  - *Supersonic 'microturbulence' vs. nonmonotonic v-fields*
  - Supersonic macro turbulence
  - (Quasi-)recombination lines
  - Optical-depth invariants and scaling relations
  - H_α in O-stars and AB-supergiants
  - Impact of wind on weaker lines, and specifically N III λ4640
  - *IR/radio excess*
  - *IR lines: inverted levels (or close to inversion)*

  - X-rays: impact on resonance lines/'superionization'
  - Emission lines in WRs
- Wind inhomogeneities/clumping
  - *Micro- and macroclumping, porosity*
  - *Clumping in RTE*
  - H_α vs. He II λ4686
  - *Velocity-porosity*
  - Clumping – coupling with rate equations
- Outlook
  - *Multi-D problems/formulation*
  - *Time dependence, relativistic treatment*
  - *Nonradial line forces (e.g., in rotating winds)*
  - *Polarization (linear, circular $\rightarrow$ B-fields)*

5.7 Appendix A: NLTE Model Atmosphere Codes for Hot Stars

Table 5.1 compares presently available atmospheric codes that can be used for the spectroscopic analysis of hot stars. Since the codes Detail/Surface and TLUSTY calculate occupation numbers/spectra within hydrostatic, plane-parallel atmospheres, they are "only" suited for the analysis of stars with negligible winds (see also end of Section 5.2). The different computation times are majorly caused by the different approaches to deal with line-blocking/blanketing. The overall agreement between the various codes (within their domain of application) is quite satisfactory, though certain discrepancies are found in specific parameter ranges, particularly regarding EUV ionizing fluxes (Puls et al., 2005; Simón-Díaz and Stasińska, 2008).

5.8 Appendix B: Further Comments on the Line Profile Function

5.8.1 *Appendix B.1: Depth Dependent Thermal Speeds*

To avoid a depth dependence of the frequency grid when measuring frequencies in depth dependent Doppler units, one uses a *fiducial* thermal speed, $v^*_{\rm th}$, such that

$$x = \frac{\nu - \tilde{\nu}}{\Delta\nu^*_{\rm D}} \quad \text{with} \quad \Delta\nu^*_{\rm D} = \frac{\tilde{\nu} v^*_{\rm th}}{c}.$$

Let

$$\delta(r) = \frac{\Delta\nu_{\rm D}(r)}{\Delta\nu^*_{\rm D}} = \frac{v_{\rm th}(r)}{v^*_{\rm th}}, \qquad \text{then} \quad \frac{\nu - \tilde{\nu} - \mu v(r)\tilde{\nu}/c}{\Delta\nu_{\rm D}(r)} = \frac{x - \mu v'(r)}{\delta(r)},$$

now with $v'(r) = v(r)/v^*_{\rm th}$ (cf. Section 5.4.1). In this notation,

$$\phi_\nu(x_{\rm CMF}, r) = \phi_\nu(x - \mu v', r) = \frac{1}{\Delta\nu^*_{\rm D}\delta(r)\sqrt{\pi}} \exp\left[-\left(\frac{x - \mu v'(r)}{\delta(r)}\right)^2\right],$$

with units "per frequency" (s), or alternatively,

$$\chi_\nu(x_{\rm CMF}, r) = \frac{\bar{\chi}_{\rm L}(r)}{\Delta\nu^*_{\rm D}} \phi(x_{\rm CMF}, r),$$

with dimensionless

$$\phi(x_{\rm CMF}, r) = \frac{1}{\delta(r)\sqrt{\pi}} \exp\left[-\left(\frac{x - \mu v'(r)}{\delta(r)}\right)^2\right], \qquad \text{and} \quad \frac{\bar{\chi}_{\rm L}(r)}{\Delta\nu^*_{\rm D}} = \frac{\bar{\chi}_{\rm L}(r)\tilde{\lambda}}{v^*_{\rm th}}.$$

TABLE 5.1. Comparison of state-of-the-art, NLTE, line-blanketed model atmosphere codes

Code	DETAIL/ SURFACE[1]	TLUSTY[2]	CMFGEN[3]	FASTWIND[4]	PHOENIX[5]	PoWR[6]	WM-basic[7]
Geometry	Plane-parallel	Plane-parallel	Spherical	Spherical	Spherical/ pl.-para./3-D	Spherical	Spherical
Blanketing	LTE	Yes	Yes	Approx.	Yes	Yes	Yes
Radiative line transfer	Observer's frame	Observer's frame	CMF	CMF/ Sobolev	CMF/ obs.frame	CMF	Sobolev
Temperature structure	Radiative equilibrium	Radiative equilibrium	Radiative equilibrium	e^- therm. balance	Radiative equilibrium	Radiative equilibrium	e^- therm. balance
Diagnostic range	No limitations	No limitations	No limitations	Optical/IR	No limitations	No limitations	UV
Major application	Hot stars with negligible winds	Hot stars with negligible winds	OB(A)-stars WRs, SNe	OB-stars, early A-sgs	Stars below 10 kK,SNe	WRs, O-stars	Hot stars w. dense winds, ion fluxes, SNe
Comments	No wind	No wind	Start model required	User-specified atomic models	Molecules included	–	No clumping
Execution time	Few minutes	Hour(s)	Hours	Few minutes to 0.5 h	Hours	Hours	1 to 2 h

[1] Giddings (1981), Butler and Giddings (1985); [2] Hubený (1998); [3] Hillier and Miller (1998); [4] Puls et al. (2005); [5] Hauschildt (1992); [6] Gräfener et al. (2002); [7] Pauldrach et al. (2001).

5.8.2 *Appendix B.2: Integrals Involving the Profile Function: Which Normalization to Use?*

- Spatial integrals of type $\int \chi^{\rm line}(\nu_{\rm CMF}, r) f_\nu(r) {\rm d}r$
$$\to \int \frac{\bar{\chi}_{\rm L}(r)}{\Delta\nu_{\rm D}} \phi(x_{\rm CMF}, r) f_\nu(r) {\rm d}r,$$
e.g., optical depth if $f_\nu(r) = 1$.
- Frequency integrals of type $\int f_\nu(r)\, \phi(\nu_{\rm CMF}, r) {\rm d}\nu$
$$\to \int f(\nu(x), r)\, \phi(x_{\rm CMF}, r) {\rm d}x,$$
e.g., scattering integrals, if $f_\nu(r) = J_\nu(r)$.
- Frequency integrals of type $\int \chi^{\rm line}(\nu_{\rm CMF}, r) f_\nu(r) {\rm d}\nu$
$$\to \bar{\chi}_{\rm L}(r) \int f(\nu(x), r)\, \phi(x_{\rm CMF}, r) {\rm d}x,$$
e.g., in the context of line acceleration, $g_{\rm rad}(r)$, see Section 5.4.3

If applicable, one needs to use $\Delta\nu_{\rm D}^*$ instead of $\Delta\nu_{\rm D}$. Moreover,

$$\phi(\nu_{\rm CMF}, r) = \frac{\phi(x_{\rm CMF}, r)}{\Delta\nu_{\rm D}}, \quad \text{i.e.,} \quad \phi(\nu_{\rm CMF}, r){\rm d}\nu = \phi(x_{\rm CMF}, r){\rm d}x,$$

and $\phi(\nu_{\rm CMF}, r) = \phi_\nu(x_{\rm CMF}, r)$ normalized with respect to frequency, whereas $\phi(x_{\rm CMF}, r)$ normalized with respect to x.

REFERENCES

Auer, L. H. and Mihalas, D. 1969. Non-LTE Model Atmospheres. III. A Complete-Linearization Method. *ApJ*, **158**(Nov.), 641.

Butler, K. and Giddings, J. R. 1985. *Newsl. Anal. Astron. Spectra*, No. 9

Cannon, C. J. 1973. Frequency-Quadrature Perturbations in Radiative-Transfer Theory. *ApJ*, **185**(October), 621–630

Castor, J. I. 1972. Radiative Transfer in Spherically Symmetric Flows. *ApJ*, **178**(December), 779–792

Castor, J. I. 1974. On the Force Associated with Absorption of Spectral Line Radiation. *MNRAS*, **169**(November), 279–306

Castor, J. I., Abbott, D. C. and Klein, R. I. 1975. Radiation-Driven Winds in Of Stars. *ApJ*, **195**(January), 157–174

Friend, D. B. and Abbott, D. C. 1986. The Theory of Radiatively Driven Stellar Winds. III Wind Models with Finite Disk Correction and Rotation. *ApJ*, **311**(December), 701–707

Friend, D. B. and Castor, J. I. 1983. Stellar Winds Driven by Multiline Scattering. *ApJ*, **272**(September), 259–272

Gabler, R., Gabler, A., Kudritzki, R. P., Puls, J. and Pauldrach, A. 1989. Unified NLTE Model Atmospheres Including Spherical Extension and Stellar Winds: Method and First Results. *A&A*, **226**(December), 162–182

Giddings, J. R. 1981. PhD Thesis, University of London

Gräfener, G., Koesterke, L. and Hamann, W. R. 2002. Line-Blanketed Model Atmospheres for WR Stars. *A&A*, **387**(May), 244–257

Hamann, W.-R. 1980. The Expanding Envelope of Zeta Puppis: A Detailed UV-Line Fit. *A&A*, **84**(April), 342–349

Hamann, W.-R. 1981. Line Formation in Expanding Atmospheres: On the Validity of the Sobolev Approximation. *A&A*, **93**(January), 353–361

Hauschildt, P. H. 1992. A Fast Operator Perturbation Method for the Solution of the Special Relativistic Equation of Radiative Transfer in Spherical Symmetry. *J. Quant. Spec. Radiat. Transf.*, **47**(6), 433–453

Hennicker, L., Puls, J., Kee, N. D. and Sundqvist, J. O. 2018. 3D Radiative Transfer: Continuum and Line Scattering in Non-Spherical Winds from OB Stars. *A&A*, **616**(September), A140

Hillier, D. J. and Miller, D. L. 1998. The Treatment of Non-LTE Line Blanketing in Spherically Expanding Outflows. *ApJ*, **496**(1), 407–427

Hubený, I. 1998. Non-LTE Line-Blanketed Model Atmospheres of Hot Stars. Page 139 of: Chan, Kwing Lam, Cheng, K. S. and Singh, H. P. (eds.), *1997 Pacific Rim Conference on Stellar Astrophysics*. Astronomical Society of the Pacific Conference Series, vol. 138

Hubený, I. and Mihalas, D. 2014. *Theory of Stellar Atmospheres*. Princeton University Press.

Hummer, D. G. and Rybicki, G. B. 1971. Radiative Transfer in Spherically Symmetric Systems: The Conservative Grey Case. *MNRAS*, **152**, 1

Hummer, D. G. and Rybicki, G. B. 1985. The Sobolev Approximation for Line Formation with Continuous Opacity. *ApJ*, **293**(June), 258–267

Kudritzki, R.-P. and Puls, J. 2000. Winds from Hot Stars. *ARA&A*, **38**, 613–666

Lamers, H. J. G. L. M., Cerruti-Sola, M. and Perinotto, M. 1987. The "SEI" Method for Accurate and Efficient Calculations of Line Profiles in Spherically Symmetric Stellar Winds. *ApJ*, **314**(March), 726–738

Lucy, L. B. 1971. The Formation of Resonance Lines in Extended and Expanding Atmospheres. *ApJ*, **163**(January), 95

Lucy, L. B. and Solomon, P. M. 1970. Mass Loss by Hot Stars. *ApJ*, **159**(March), 879–893

Mihalas, D. 1978. *Stellar Atmospheres*, 2nd edition W. H. Freeman and Co.

Mihalas, D., Kunasz, P. B. and Hummer, D. G. 1975. Solution of the Comoving Frame Equation of Transfer in Spherically Symmetric Flows. I Computational Method for Equivalent-Two-Level-Atom Source Functions. *ApJ*, **202**(December), 465–489

Mihalas, D., Kunasz, P. B. and Hummer, D. G. 1976. Solution of the Comoving-Frame Equation of Transfer in Spherically Symmetric Flows. III. Effect of Aberration and Advection Terms. *ApJ*, **206**(June), 515–524

Olson, G. L., Auer, L. H. and Buchler, J. R. 1986. A Rapidly Convergent Iterative Solution of the Non-LTE Line Radiation Transfer Problem. *J. Quant. Spec. Radiat. Transf.*, **35**(June), 431–442

Owocki, S. P. and Puls, J. 1996. Nonlocal Escape-Integral Approximations for the Line Force in Structured Line-driven Stellar Winds. *ApJ*, **462**(May), 894

Owocki, S. P. and Puls, J. 1999. Line-Driven Stellar Winds: The Dynamical Role of Diffuse Radiation Gradients and Limitations to the Sobolev Approach. *ApJ*, **510**(January), 355–368

Owocki, S. P. and Rybicki, G. B. 1984. Instabilities in Line-Driven Stellar Winds. I Dependence on Perturbation Wavelength. *ApJ*, **284**(September), 337–350

Pauldrach, A., Puls, J. and Kudritzki, R. P. 1986. Radiation-Driven Winds of Hot Luminous Stars: Improvements of the Theory and First Results. *A&A*, **164**(August), 86–100

Pauldrach, A. W. A., Hoffmann, T. L. and Lennon, M. 2001. Radiation-Driven Winds of Hot Luminous Stars. XIII. A Description of NLTE Line Blocking and Blanketing towards Realistic Models for Expanding Atmospheres. *A&A*, **375**(August), 161–195

Puls, J. 1987. Radiation-Driven Winds of Hot Luminous Stars. IV The Influence of Multi-Line Effects. *A&A*, **184**(October), 227–248

Puls, J. 1991. Approximate Lambda-Operators Working at Optimum Convergence Rate. II Line Transfer in Expanding Atmospheres. *A&A*, **248**(August), 581–589

Puls, J. and Herrero, A. 1988. Approximate Lambda-Operators Working at Optimum Convergence Rate. I Theory and Application to Hydrostatic Atmospheres. *A&A*, **204**(October), 219–228

Puls, J. and Hummer, D. G. 1988. The Sobolev Approximation for the Line Force and Line Source Function in a Spherically-Symmetrical Stellar Wind with Continuum Opacity. *A&A*, **191**(February), 87–98

Puls, J., Owocki, S. P. and Fullerton, A. W. 1993. On the Synthesis of Resonance Lines in Dynamical Models of Structured Hot-Star Winds. *A&A*, **279**(November), 457–476

Puls, J., Urbaneja, M. A., Venero, R., Repolust, T., Springmann, U., Jokuthy, A. and Mokiem, M. R. 2005. Atmospheric NLTE-Models for the Spectroscopic Analysis of Blue Stars with Winds. II. Line-Blanketed Models. *A&A*, **435**(May), 669–698

Puls, J., Vink, J. S. and Najarro, F. 2008. Mass loss from hot massive stars. *A&A Rev.*, **16**(Dec.), 209–325.

Rybicki, G. B. 1991 (Jan). Recent Advances in Computational Methods. Page 1 of: Crivellari, L., Hubený, I. and Hummer, D. G. (eds.), *NATO Advanced Science Institutes (ASI)* Series C, vol. 341.

Rybicki, G. B., and Hummer, D. G. 1978. A generalization of the Sobolev method for flows with nonlocal radiative coupling. *ApJ*, **219**(Jan.), 654–675.

Rybicki, G. B., and Hummer, D. G. 1991. An accelerated lambda iteration method for multilevel radiative transfer. I - Non-overlapping lines with background continuum. *A&A*, **245**(May), 171–181.

Santolaya-Rey, A. E., Puls, J., and Herrero, A. 1997. Atmospheric NLTE-models for the spectroscopic analysis of luminous blue Stars with Winds. *A&A*, **323**(July), 488–512.

Simón-Díaz, S. and Stasińska, G. 2008. The Ionizing Radiation from Massive Stars and Its Impact on HII Regions: Results from Modern Model Atmospheres. *MNRAS*, **389**(September), 1009–1021

Sobolev, V. V. 1957. The Diffusion of Lα Radiation in Nebulae and Stellar Envelopes. *Soviet Ast.*, **1**(October), 678

Sobolev, V. V. 1960. *Moving Envelopes of Stars*. Harvard University Press

Taresch, G., Kudritzki, R. P., Hurwitz, M., et al. 1997. Quantitative Analysis of the FUV, UV and Optical Spectrum of the O3 Star HD 93129A. *A&A*, **321**(May), 531–548

Trujillo Bueno, J. and Fabiani Bendicho, P. 1995. A Novel Iterative Scheme for the Very Fast and Accurate Solution of Non-LTE Radiative Transfer Problems. *ApJ*, **455**(December), 646

Werner, K. and Husfeld, D. 1985. Multi-Level Non-LTE Line Formation Calculations Using Approximate Lambda-Operators. *A&A*, **148**(July), 417–422